

AFML-TR-69-117
PART III

AD709946

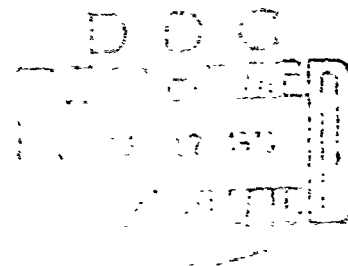
**PHASE EQUILIBRIA INVESTIGATIONS OF
BINARY, TERNARY, AND HIGHER
ORDER SYSTEMS**

PART III. PHASE EQUILIBRIA STUDIES IN THE Nb-Ta-C SYSTEM

P. BOOKER and E. RUDY

TECHNICAL REPORT AFML-TR-69-117, PART III

MAY 1970



This document has been approved for public release and sale;
its distribution is unlimited

AIR FORCE MATERIALS LABORATORY
AIR FORCE SYSTEMS COMMAND
WRIGHT-PATTERSON AIR FORCE BASE, OHIO

68

NOTICES

When Government drawings, specifications, or other data are used for any purpose other than in connection with a definitely related Government procurement operation, the United States Government thereby incurs no responsibility nor any obligation whatsoever, and the fact that the Government may have formulated, furnished, or in any way supplied the said drawings, specifications, or other data, is not to be regarded, by implication or otherwise, as in any manner licensing the holder or any other person or corporation, or conveying any rights or permission to manufacture, use, or sell any patented invention that may in any way be related thereto. This document has been approved for public release and sale; its distribution is unlimited.

ACCESSION FOR	
CPSTI	WHITE SECTION <input checked="" type="checkbox"/>
DBC	BLUE SECTION <input type="checkbox"/>
UNANNOUNCED <input type="checkbox"/>	
JUSTIFICATION	
BY	
DISTRIBUTION AVAILABILITY CODE	
REST.	AVAIL. and/or SPECIAL
1	

Copies of this report should not be returned unless return is required by security consideration, contractual obligations, or notice on a specific document.

**PHASE EQUILIBRIA INVESTIGATIONS OF
BINARY, TERNARY, AND HIGHER
ORDER SYSTEMS**

PART III. PHASE EQUILIBRIA STUDIES IN THE Nb-Ta-C SYSTEM

P. BOOKER and E. RUDY

**This document has been approved for public release and sale;
its distribution is unlimited.**

FOREWORD

The experimental research described in this technical report was carried out at the Materials Research Laboratory, Aerojet-General Corporation, Sacramento, California, under USAF Contract F33615-67-C-1513, Project 7350, Task 735001. The contract was administered under the direction of the Air Force Materials Laboratory (MAMC), with Capt. P. J. Marchiando, as Project Engineer, and Dr. E. Rudy, Aerojet-General Corporation (now at the Oregon Graduate Center, Portland, Oregon) serving as Principal Investigator.

The authors wish to acknowledge the help of Messrs J. Pomodoro (fabrication of samples), and of R. Crisloni, who prepared the drawings.

The manuscript of this report was released by the authors March 1970 for publication.

Other reports issued, or in preparation, under USAF Contract F33615-67-C-1513, include:

- Part I. The Phase Diagrams of the Systems Ti-Nb-C, Ti-Ta-C, and Ti-Mo-C
- Part II. Effect of Re and Al Additions on the Metal-Rich Phase Equilibria in the Ti-Mo-C and Ti-Nb-C Systems.

This technical report has been reviewed and is approved.



W. G. Ramke
Chief, Ceramics and Graphite Branch
Metals and Ceramics Division
Air Force Materials Laboratory

ABSTRACT

The solid state and solid-liquid equilibria of the Nb-Ta-C system have been determined by melting point determinations, X-ray and chemical analysis, metallography, and differential thermal analysis for temperatures above 1500°C.

The ternary system has a complete solid solution of monocarbides and also of subcarbides if the difference in carbon atom ordering is disregarded. Eutectic troughs in both the metal-rich and carbon-rich regions of the ternary are present. Calculated tie-line distributions agree well with experimental results.

TABLE OF CONTENTS

	<u>Page</u>
I. Introduction and Summary	1
A. Introduction	1
B. Summary	1
II. Literature Review	5
A. The Tantalum-Niobium System	5
B. The Niobium-Carbon System	6
C. The Tantalum-Carbon System	7
D. The Niobium-Tantalum-Carbon System	8
III. Experimental Program	9
A. Starting Materials	9
B. Alloy Preparation and Heat Treatments	10
C. Determination of Melting Points	12
D. Differential Thermal Analysis (DTA)	13
E. Metallography	14
F. X-Ray Analysis	14
G. Chemical Analysis	15
IV. Experimental Results	16
A. The Tantalum-Niobium Binary System	16
B. Solid State Phase Equilibria in the Ternary Nb-Ta-C System	17
C. Phase Equilibria at High Temperature	27
D. Assembly of the Phase Diagram	42
V. Conclusions and Discussion	49
References	55

ILLUSTRATIONS

FIGURE		PAGE
1.	Nb-Ta: Phase Diagram	1
2.	Nb-Ta-C: Constitution Diagram	3
3.	Nb-Ta-C: Scheil-Schulz Reaction Diagram	3
4.	Nb-Ta-C: Liquidus Projections	4
5.	Nb-Ta-C: Isopleth at 32.5 Atomic % Carbon	4
6.	Nb-Ta: Phase Diagram	5
7.	Nb-C: Phase Diagram	6
8.	Ta-C: Phase Diagram	7
9.	Nb-Ta-C: Compositions of Melting Point Samples	11
10.	Nb-Ta-C: Compositions of Alloys Investigated by Differential Thermal Analysis	12
11.	Nb-Ta-C: Compositions of Solid-State Samples Heat-Treated at 1500 and 1800°C	13
12.	Nb-Ta: Melting Temperatures	16
13.	Nb-Ta-C: Qualitative X-Ray Evaluation of Alloys Equilibrated at 1800°C	17
14.	Nb-Ta-C: Qualitative X-Ray Evaluation of Alloys Equilibrated at 1500°C	18
15.	Nb-Ta-C: Lattice Parameters of the Ternary Monocarbide Solid Solutions	19
16.	Nb-Ta-C: Lattice Parameters of the Ternary Subcarbide Solid Solutions	20
17.	Nb-Ta-C: Order-Disorder Phase Reaction of Nb ₂ C and Ta ₂ C in Ternary Alloys	22
18.	Nb-Ta-C: Photomicrograph of a DTA Sample (47/20/33 At. %)	23
19.	Nb-Ta-C: Photomicrograph of a DTA Sample (55/12/33 At. %)	24

ILLUSTRATIONS (Cont)

FIGURE		PAGE
20.	Nb-Ta-C: α - β -Nb ₂ C Phase Reaction in Ternary Alloys	25
21.	Nb-Ta-C: Photomicrograph of a DTA Sample (55/12/33 At. %)	26
22.	Nb-Ta-C: Photomicrograph of a DTA Sample (62/5/33 At. %)	27
23.	Nb-Ta-C: Photomicrograph of an Arc-Melted Sample (49/49/2 At. %)	28
24.	Nb-Ta-C: Photomicrograph of an Arc-Melted Sample (48/47/5 At. %)	29
25.	Nb-Ta-C: Photomicrograph of an Arc-Melted Sample (46/46/8 At. %)	29
26.	Nb-Ta-C: Melting Temperatures and Location of the Metal-Rich Eutectic Trough Between (Nb, Ta) and (Nb, Ta) ₂ C	30
27.	Nb-Ta-C: Photomicrograph of an Arc-Melted Sample (75/14/11 At. %)	31
28.	Nb-Ta-C: Photomicrograph of an Arc-Melted Sample (30/59/11 At. %)	31
29.	Nb-Ta-C: Photomicrograph of an Arc-Melted Sample (15/73/12 At. %)	32
30.	Nb-Ta-C: Photomicrograph of a DTA Sample (62/10/28 At. %)	33
31.	Nb-Ta-C: Photomicrograph of a DTA Sample (32/40/28 At. %)	33
32.	Nb-Ta-C: Peritectic Melting Temperatures of the Solid Solution (Nb, Ta) ₂ C	34
33.	Nb-Ta-C: Photomicrograph of a Melting Point Sample (60/5/35 At. %)	35
34.	Nb-Ta-C: Photomicrograph of a Melting Point Sample (47/18/35 At. %)	36
35.	Nb-Ta-C: Maximum Solidus Temperatures of the Ternary Monocarbide Phase	37

ILLUSTRATIONS (Cont)

FIGURE		PAGE
36.	Nb-Ta-C: Photomicrograph of a Melting Point Sample (16/43/47 At. %)	38
37.	Nb-Ta-C: Photomicrograph of a Melting Point Sample (25/30/45 At. %)	38
38.	Nb-Ta-C: Photomicrograph of a Melting Point Sample (40/15/45 At. %)	39
39.	Nb-Ta-C: Experimental Solidus Temperatures and Location of the Eutectic Trough Between the Monocarbide Solid Solution and Graphite	40
40.	Nb-Ta-C: Photomicrograph of a Melting Point Sample (11/28/61 At. %)	41
41.	Nb-Ta-C: Photomicrograph of a Melting Point Sample (33/6/61 At. %)	41
42-53	Nb-Ta-C: Isothermal Sections at 1500, 1800, 2200, 2400, 2600, 2900, 3200, 3320, 3440, 3600, 3650, and 3800°C	42-48
54.	Nb-Ta-C: Liquidus Projections	48
55.	Nb-Ta-C: Schematic Illustration for the Formation of the γ -(Nb, Ta) ₂ C _{1+x} Phase	50
56.	Nb-Ta-C: Calculated Section at 1800°C	53
57.	Nb-Ta-C: Calculated Section at 1500°C	54

TABLES

TABLE		PAGE
1	Structure and Lattice Parameters of Niobium and Tantalum Carbides	8
2	Carbon Analyses and Lattice Parameters of Carbide Starting Materials	10
3	Free Enthalpy Data of Niobium Carbides	51
4	Free Enthalpy Data of Tantalum Carbides	51

I. INTRODUCTION AND SUMMARY

A. INTRODUCTION

The continuing work on the delinearization of the high-temperature phase equilibria of binary, ternary, and higher order refractory metal-carbide, boride, nitride, and silicide systems is directed in this report to the study of the Nb-Ta-C system with the expressed purpose of using the data generated for possible applications in the field of new cutting tools containing refractory metal alloys as a binder phase.

B. SUMMARY

Figure 1 shows results of the new investigations in Nb-Ta binary system; the narrow two-phase region of liquid and melt has been confirmed.

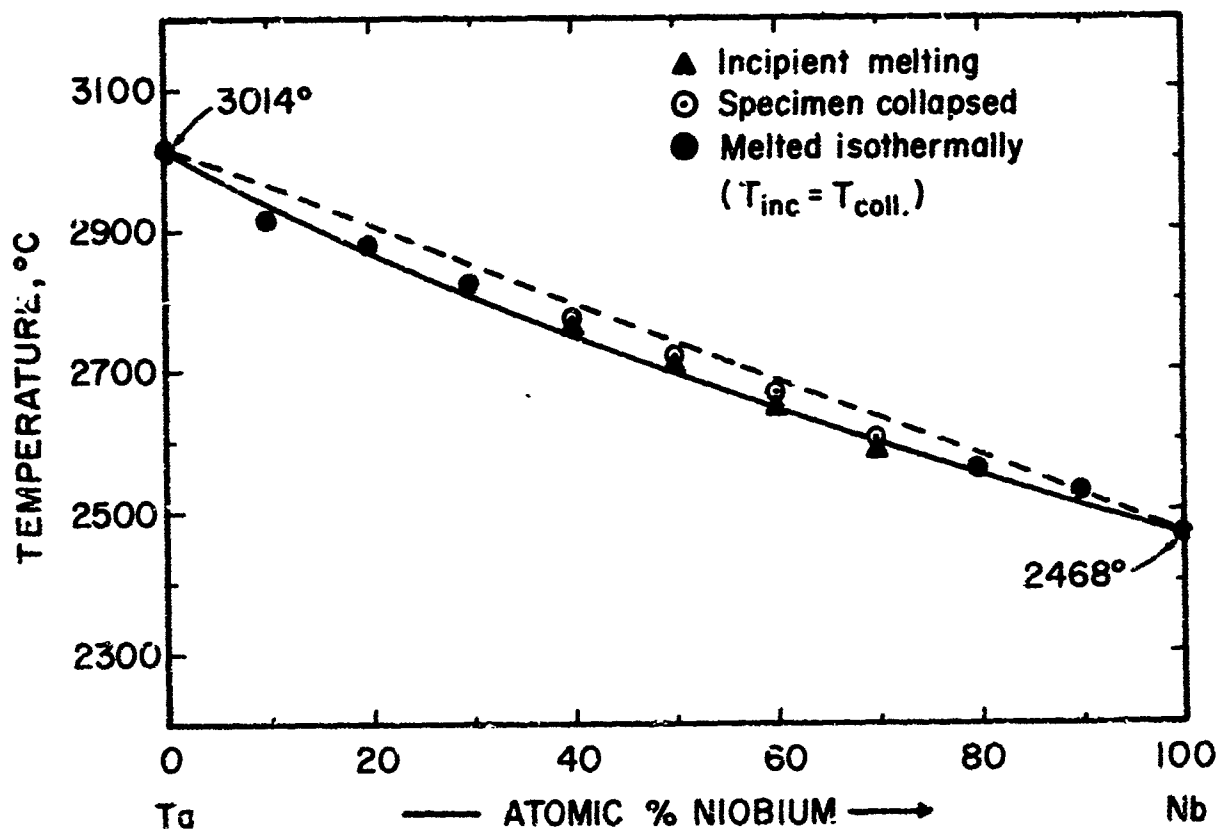


Figure 1. Nb-Ta: Phase Diagram

The phase equilibria in the niobium-tantalum-carbon system are summarized as follows:

The monocarbides, TaC and NbC form a continuous series of solid solutions from 1500°C to melting. With disregard of the fact that the low temperature forms of Ta₂C(α) and Nb₂C(β) have different ordering of carbon atoms, lattice parameter variations that are based on the L'3 lattice (random orientation assumed), show that the subcarbides Nb₂C and Ta₂C form a complete series of solid solutions.

The peritectic decomposition temperatures of the binary subcarbide solid solution varies smoothly across the ternary region, while the maximum melting temperature of the tantalum monocarbide solid solution drops rather quickly with small niobium additions.

Both the metal-rich and carbon-rich regions of this ternary are further characterized by the presence of eutectic troughs running across the ternary region and join the respective binary metal-subcarbide and monocarbide-graphite eutectics.

Thermodynamic calculations yielding the tie line positioning in the two-phased regions metal + subcarbide and subcarbide + monocarbide show that these values compare quite well with the experimentally determined tie lines.

The isometric view of the ternary phase diagram, shown for temperatures above 1500°C (Figure 2) is supplemented by the flow diagram of binary and ternary reactions (Figure 3) as well as the liquidus projections (Figure 4). An isopleth at 32.5% carbon is shown in Figure 5.

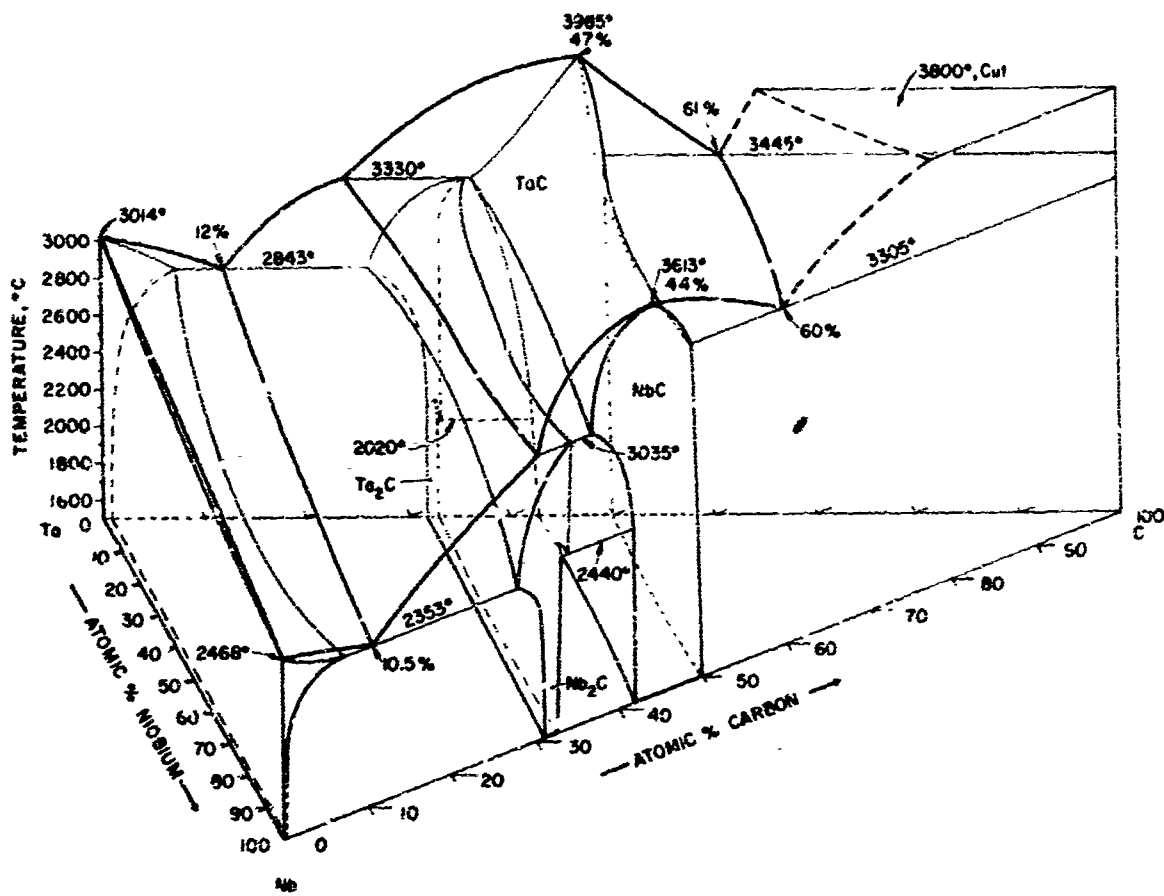


Figure 2. Nb-Ta-C: Constitution Diagram

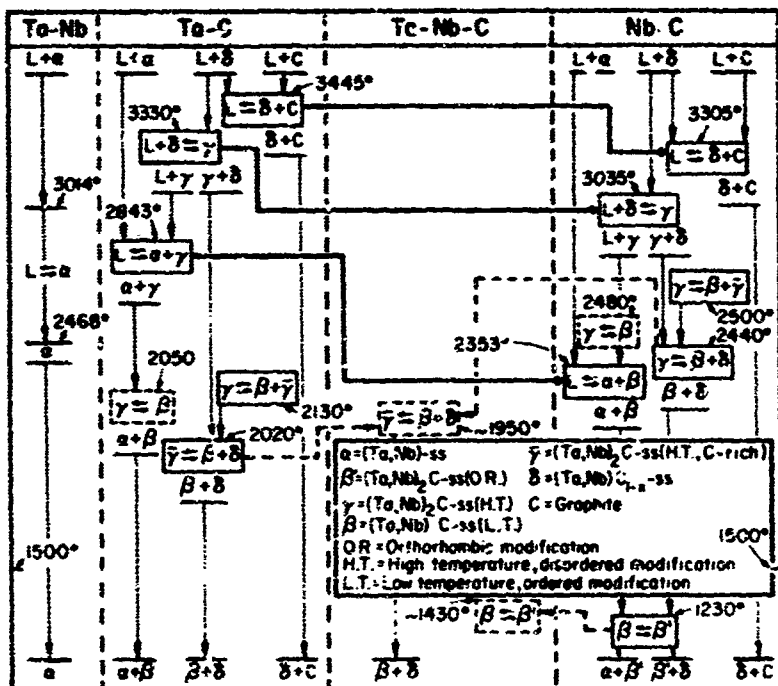


Figure 3. Nb-Ta-C: Scheil-Schulz Reaction Diagram

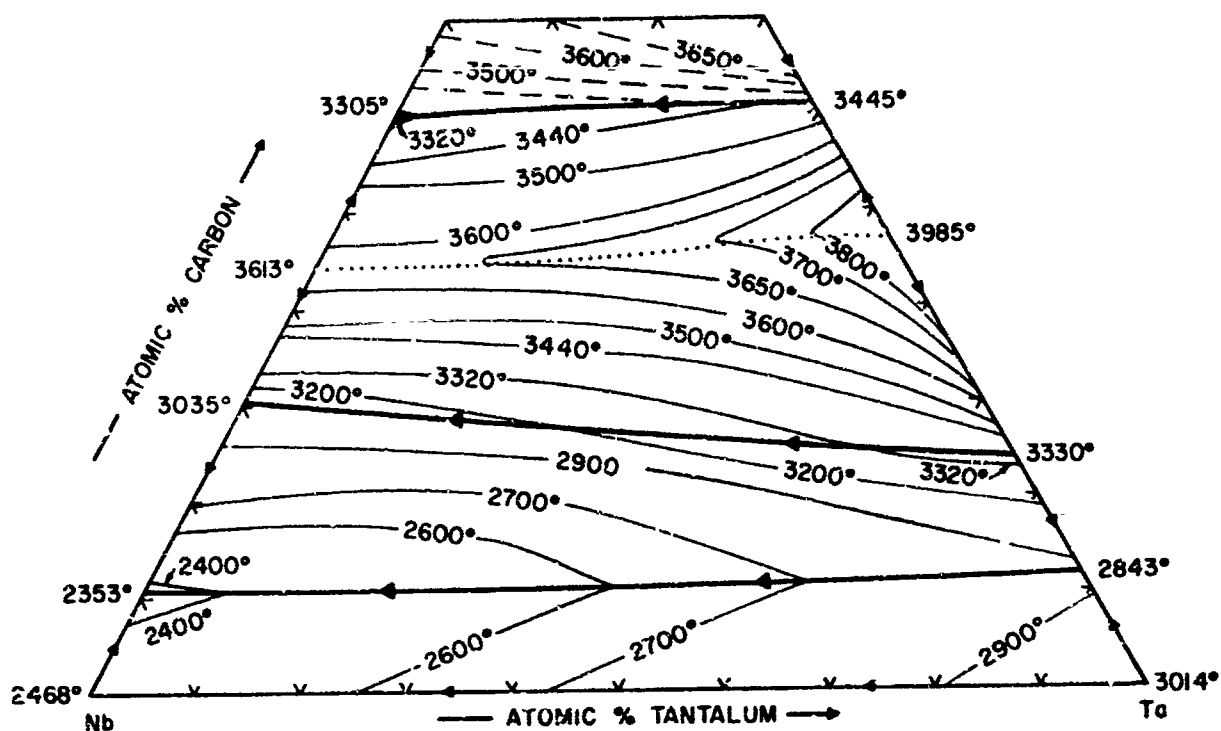


Figure 4. Nb-Ta-C: Liquidus Projections

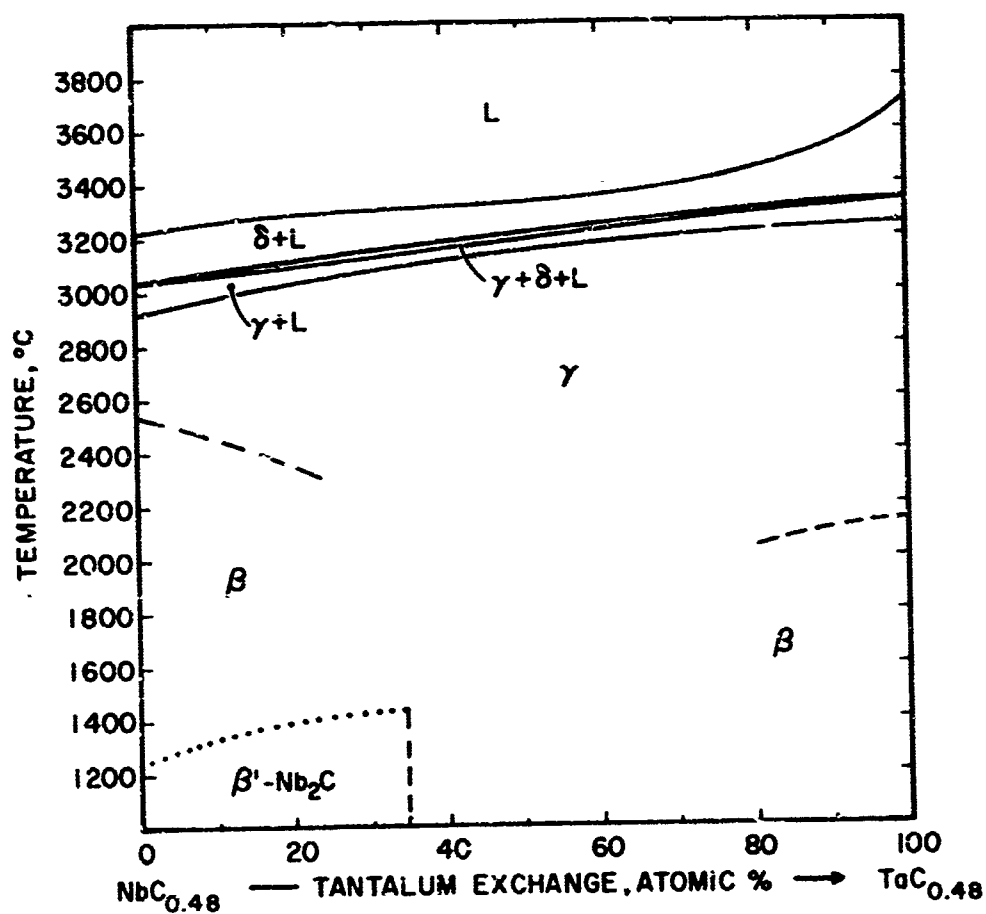


Figure 5. Nb-Ta-C: Isopleth at 32.5 Atomic % Carbon

II. LITERATURE REVIEW

A. THE TANTALUM-NIOBIUM SYSTEM

These two metals form a continuous series of solid solutions in the body centered cubic structure⁽¹⁾; the phase diagram was determined by Williams and Pechin⁽²⁾; the constitution diagram, showing the smooth variation in solidus temperatures, is given in Figure 6.

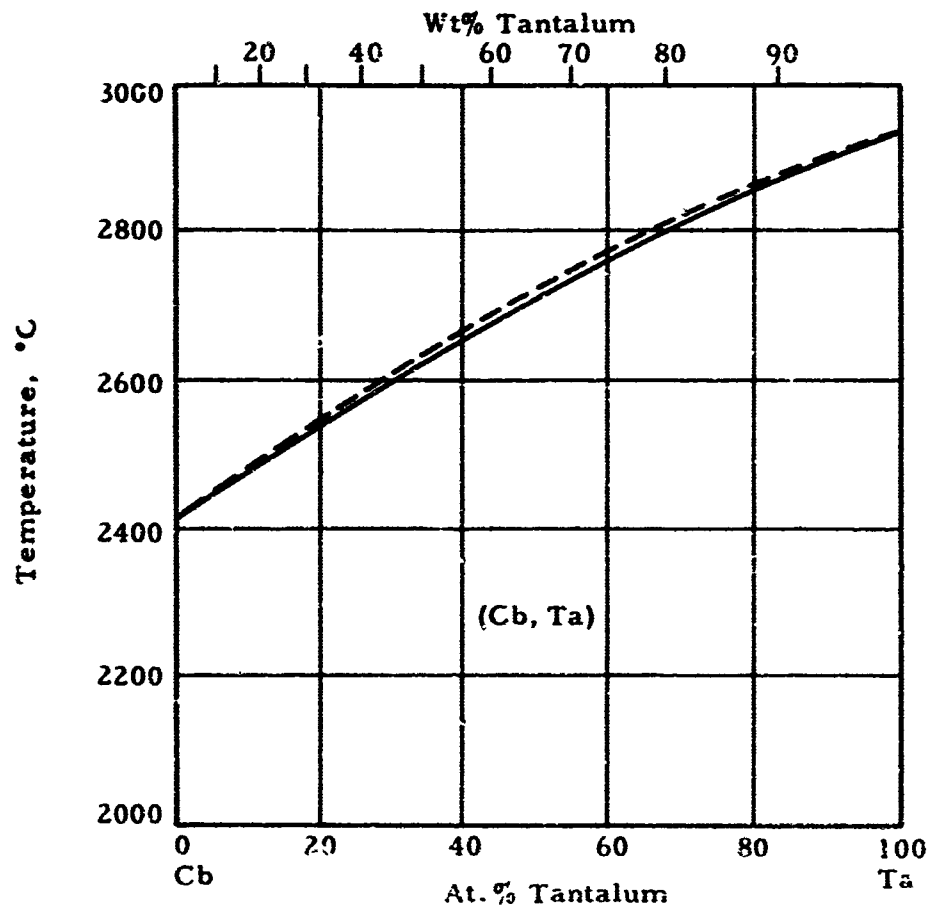


Figure 6. Nb-Ta: Phase Diagram⁽²⁾

B. THE NIOBIUM-CARBON SYSTEM

The investigations of the niobium-carbon system by E. K. Storms and N. H. Krikorian⁽³⁾ and H. Kimura and Y. Sasaki⁽⁴⁾ were recently supplemented by E. Rudy, et al.^(5, 6). The system, Figure 7, contains a very refractory monocarbide with the B-1 structure (Table 1) and a subcarbide, which exists in at least two different states of sublattice order at low temperatures⁽⁵⁻¹¹⁾, and in a disordered state above approximately 2500°C⁽⁶⁾. The melting point measurements by E. Rudy, et al.⁽⁵⁾ are in close confirmation of the data by H. Kimura and Y. Sasaki⁽⁴⁾.

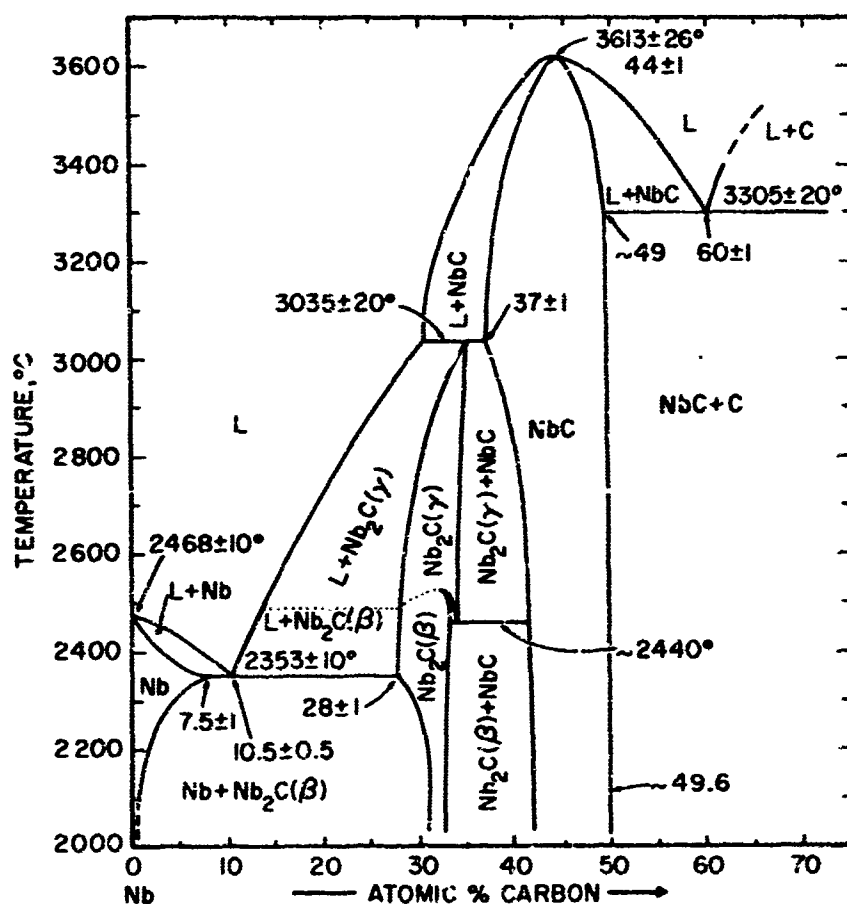


Figure 7. Nb-C: Phase Diagram^(5, 6)

C. THE TANTALUM-CARBON SYSTEM

The most recent phase diagram⁽¹²⁾ of the tantalum-carbon system is shown in Figure 8. The system contains an extremely refractory, cubic monocarbide and a peritectically decomposing, hexagonal subcarbide. The ordered, low-temperature modification of Ta_2C ⁽¹³⁾ transforms at temperatures between 2100 and 2200°C⁽¹²⁾ into another modification, which is characterized by the absence of long-range order in the carbon sublattice. With the exception of the displacive transformation, which is absent in Ta_2C , the transformation characteristics are similar to that of Mo_2C . Another phase, ζ , reported to occur in the vicinity of 40 At. % carbon⁽¹⁴⁾, was indicated to be only metastable^(12, 15); the latter viewpoint, however, was disputed in more recent work⁽¹⁶⁾. A compilation of structural data as well as of lattice parameters for the tantalum carbides is also contained in Table 1.

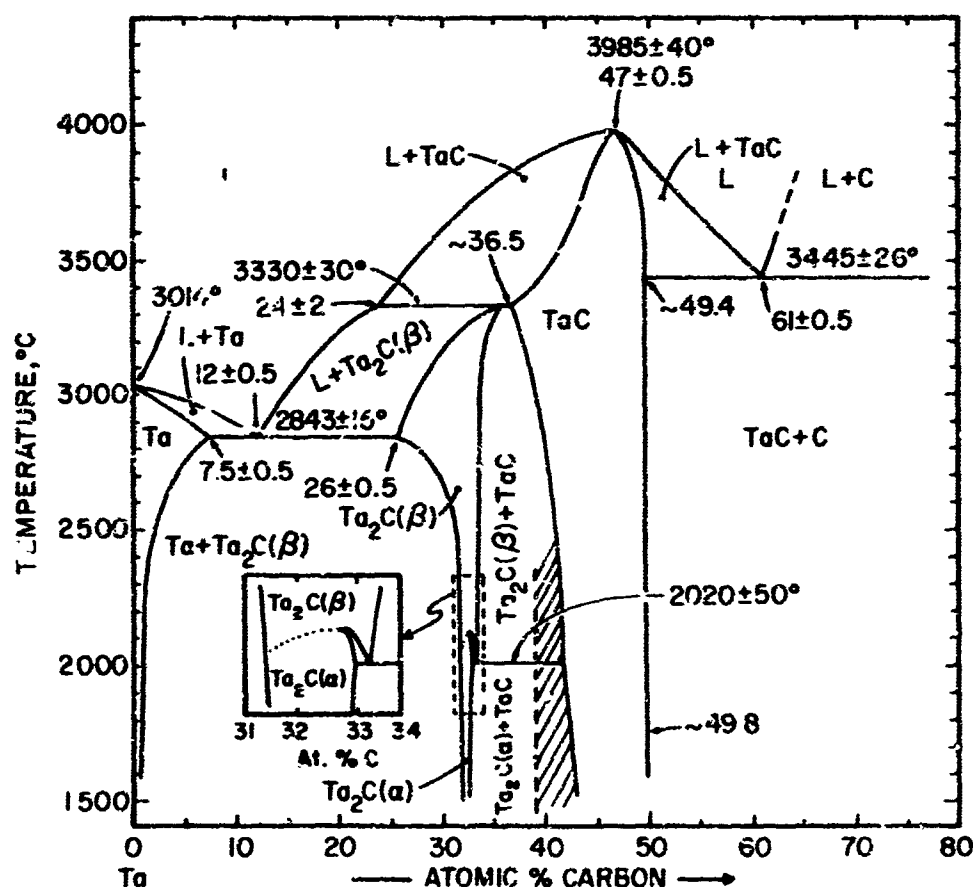


Figure 8. Ta-C: Phase Diagram⁽¹²⁾. Shaded Area Shows the Range of the Metastable ζ -Phase

Table 1. Structure and Lattice Parameters of Niobium and Tantalum Carbides

Phase	Structure	Lattice Parameters, Angstrom
Nb ₂ C	1. T < 1200°C Orthorh.	a=12.36, b=10.85 ₅ , c=4.968 ^{(6,11)(*)} a=10.92, b=4.974, c=3.90 ^{(10)(**)} a=5.40 ₇ , c=4.960 ^{(7)(***)}
	2. 1200 to 2500°C Probably hex. ε-Fe ₂ N-type	
	3. T > 2500°C Hex. approach L'3-type	a=3.125 c=4.972 at 33.3 At.%C ⁽³⁾
NbC	Fcc., B1-type	a=4.431 at 41.5 At.%C a=4.470 at ~ 50 At.%C ⁽⁷⁾
Ta ₂ C	1. T < 2000-2150°C Hex., C6-type	a=3.103; c=4.938 at 33 At.%C ⁽¹³⁾ a=3.100; c=4.931 at 31.5 At.%C a=3.102; c=4.940 at 33 At.%C ⁽¹²⁾
	2. T > 2150°C: Hex., L'3-type (no long-range order in carbon sublattice)	L'3-type cannot be retained by quenching; parameters comparable to those of the ordered modification.
TaC	Fcc., B1-type	a=4.411 at 42.5 At.%C a=4.4545 at ~ 50 At.%C ⁽¹⁴⁾
<p>* The orthorhombic axes are related to the (distorted) hexagonal subcell by:</p> $a_{o.r.} \sim 4a_{hex}; b_{o.r.} \sim 2a_{hex} \sqrt{3}; c_o = c_{hex}$ <p>** $a_{o.r.} \simeq 2a_{hex} \sqrt{3}; b_{o.r.} = c_{hex}; c_{o.r.} \simeq a_{hex}$</p> <p>*** $a = a_{hex. subcell} \sqrt{3}; c = c_{subcell}$</p> <p>+ $a_{o.r.} = c_{hex}; b_{o.r.} \simeq 2a_{hex}; c_{o.r.} = a_{hex} \sqrt{3}$</p>		

D. THE NIOBIUM-TANTALUM-CARBON SYSTEM

The continuous solid solution of NbC and TaC was established by Nowotny and Pfeiffer⁽¹⁷⁾ and confirmed by Norton and Mowry⁽¹⁸⁾. The melting points of the NbC-TaC solid solution, showing a smooth variation, were determined by Agte and Alterthum⁽¹⁹⁾.

III. EXPERIMENTAL PROGRAM

A. STARTING MATERIALS

The elemental powders, as well as alloys consisting of Nb_2C , NbC , Ta_2C , and TaC , served as the starting materials for the preparation of the experimental alloys.

Niobium metal powder was purchased from the Wah Chang Corporation, Albany, Oregon. The powder had the following main impurities (in ppm): O-730, N-45, H-80, C-30, Ta-500, Zr-200, and the sum of other metallic impurities-500.

Tantalum metal powder, also purchased from the Wah Chang Corporation, Albany, Oregon, had the following main impurities (in ppm): Al-22, C-170, Cr-20, Cu-40, Fe-210, H-40, W-64, O-590, Si-40, Ti-20, W-27, Nb-100. The lattice parameter of this starting material was $a = 3.303 \text{ \AA}$.

The Wah Chang Corporation, Albany, Oregon, supplied the tantalum monocarbide. The main impurities were (in ppm): Al-20, Nb-420, Cr-300, Cu-20, Si-10, Ti-14, Zn-10, (O-280). * The monocarbide had a carbon content of 6.11% (49.5 At.%). * The particle size was less than 15μ ; the lattice parameter of this starting material was $a = 4.455 \text{ \AA}$.

The spectrographic-grade graphite powder was purchased from the Union Carbide Corporation, Carbon Products Division, and had the following main impurities (in ppm): S-110, Si-46, Cu-44, Fe-40, Al-8, Ti-4, Mg-2, V-trace, and ash-800 maximum. The particle size was 99% smaller than 74μ . No second phase impurities were detected in highly overexposed X-ray films.

*The chemical analysis of the starting materials was performed at the Quality Control Division, Aerojet-General Corporation.

The carbide master alloys of Nb_2C , NbC , and Ta_2C were prepared by reacting the carefully blended and cold-pressed mixtures of the metal powders and carbon in a graphite-element furnace. The niobium carbides were made under vacuum (4 hr at 1900°C , $< 5 \times 10^{-5}$ Torr) while the tantalum subcarbide was reacted for 4 hours at 2000°C under a vacuum of better than 2×10^{-5} Torr. The reacted powders were crushed and comminuted to a smaller grain size than 60μ . The powders were leached in a hot 2N mixture of hydrochloric and sulfuric acid, the slurry centrifuged, washed with ether, and then dried in vacuum. The carbon and X-ray analyses of the carbide powders are listed in Table 2.

Table 2. Carbon Analyses and Lattice Parameter of Carbide Starting Materials

Carbide	Carbon Content, At. %	Phases Present	Lattice Parameters, Å
Nb_2C	33.2 ± 0.2	Nb_2C + trace NbC	$a = 3.124$; $c = 4.963$
NbC	49.2 ± 0.2	NbC	$a = 4.470$
Ta_2C	33.0 ± 0.2	Ta_2C + slight trace TaC	$a = 3.102$; $c = 4.940$

B. ALLOY PREPARATION AND HEAT TREATMENTS

Separate series of alloys were prepared for melting point, DTA, as well as for studies of the solid state section of the system.

The majority of the alloy samples were prepared by short-duration hot-pressing⁽²⁰⁾ of the well-mixed powder mixtures in graphite dies. After hot-pressing, the specimens were surface-ground to remove the reaction zone and traces of adhering graphite.

To eliminate the possibility for carbon contamination, melting point alloys from the binary system Nb-Ta were cold-pressed and high vacuum-sintered (1 hr at 1550°C) prior to the melting point runs. The DTA specimens were used in the as-hot-pressed state, but received a homogenization treatment in the DTA furnace prior to making the runs.

For metallographic investigation, selected melting point specimens from the concentration areas around the eutectic troughs were examined. Wherever the melting point samples were too porous for metallographic examination, they were arc-melted in a nonconsumable tungsten electrode melting furnace under a high-purity helium atmosphere.

Nine melting point alloys were prepared to determine the maximum solidus temperatures of the Nb-Ta binary, and the melting temperatures of the ternary alloys were determined using 45 different alloy compositions (Figure 9).

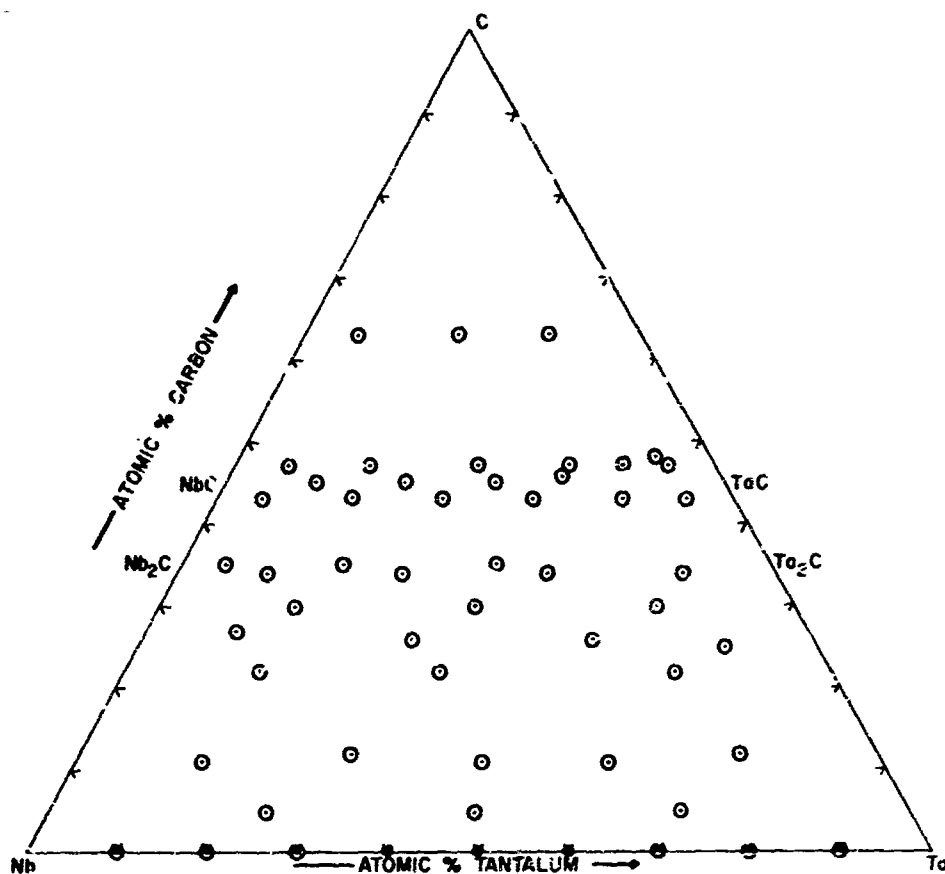


Figure 9. Nb-Ta-C: Compositions of Melting Point Samples

For the DTA studies, a total of 12 alloys were prepared and machined to the required size⁽²⁰⁾. The DTA specimens were located between the subcarbides of niobium and tantalum (Figure 10).

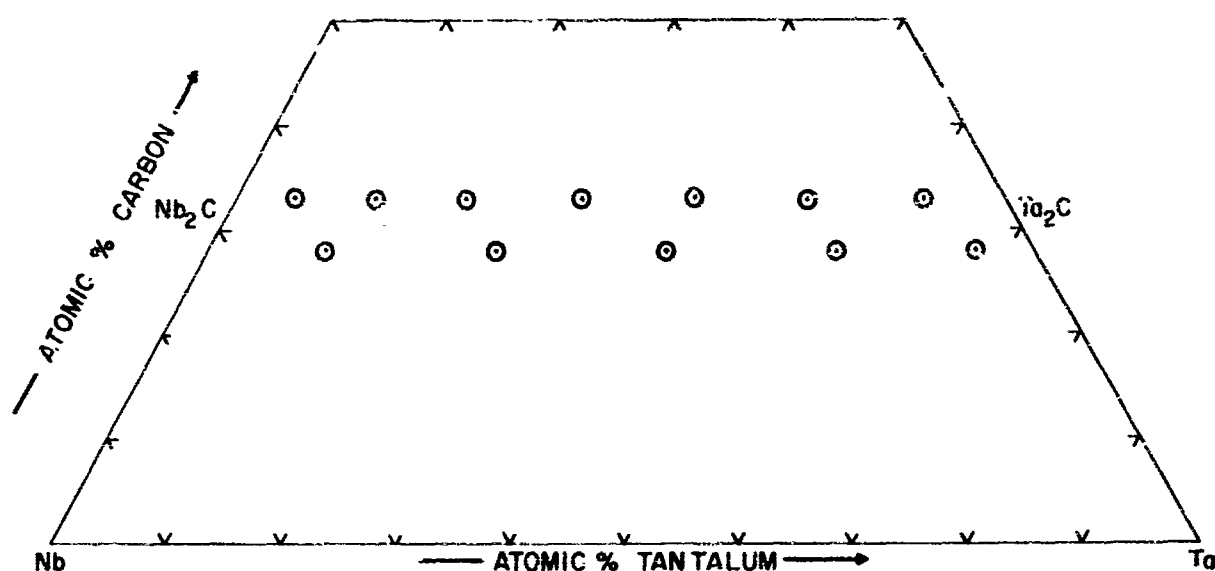


Figure 10. Nb-Ta-C: Compositions of Alloys Investigated by Differential Thermal Analysis

A total of 39 alloys were prepared for the solid state investigation of the system. The alloys having carbon compositions greater than 34 At. % C were heat treated at 1800°C for 64 hr, and selected alloys were also heat treated at 1500°C for 64 hr as shown in Figure 11. Both heat treatments were carried out in a tungsten mesh element furnace (R. Brew Company) under a high-purity helium atmosphere.

C. DETERMINATION OF MELTING POINTS

The melting points of the ternary alloys were determined by the previously described Pirani-technique^(20, 21). To minimize the carbon losses at the high melting temperatures in the monocarbide region, the melting point furnace was pressurized with high purity helium to 2-1/4 atmospheres after a short degassing of the sample under a 30-in. Hg vacuum at about 2000°C.

The temperature measurements were carried out with a disappearing filament micropyrometer, which was calibrated against a certified

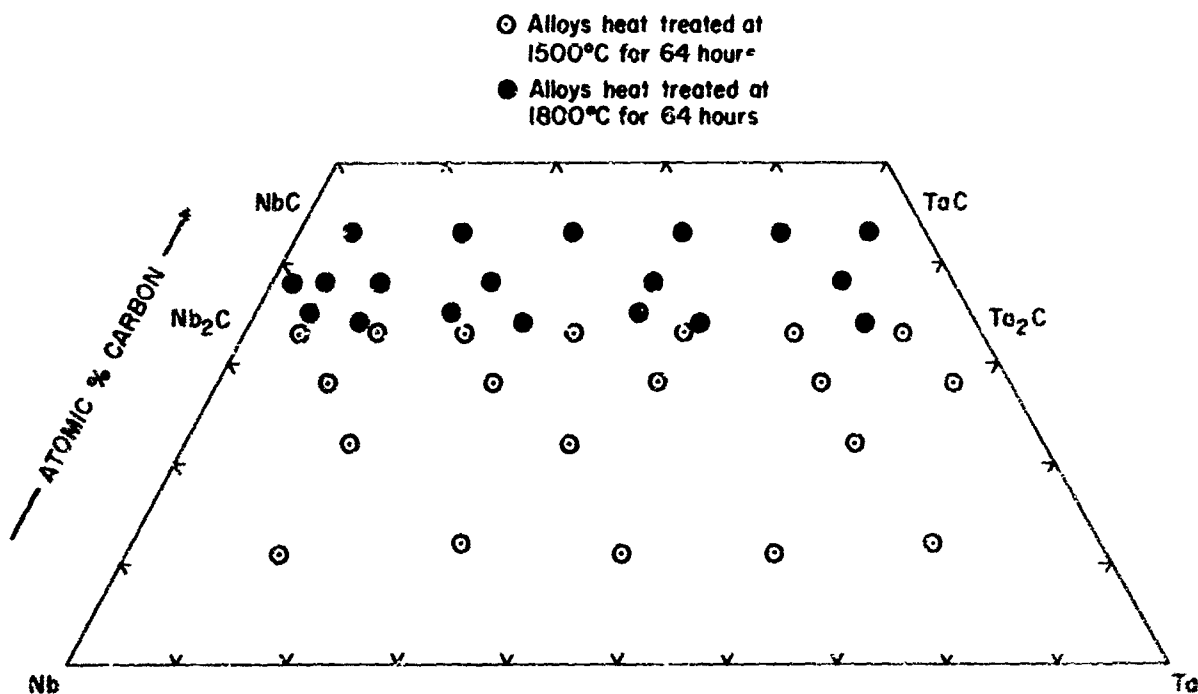


Figure 11. Nb-Ta-C: Compositions of Solid State Samples Heat-Treated at 1500°C and 1800°C

lamp from the National Bureau of Standards. The temperature was corrected for absorption losses in the quartz window of the melting point furnace and deviations due to non-black-body conditions of the observation hole. The detailed treatment with regard to the temperature corrections has been described in previous reports^(20,21).

D. DIFFERENTIAL THERMAL ANALYSIS (DTA)

The DTA specimens were run under a protective, high-purity helium atmosphere at 2 atmospheres pressure. The details of the DTA apparatus have been presented in earlier publications^(20,22)

The effect of tantalum upon the α - β Nb₂C transformation was investigated by this technique. The DTA measurements also yielded information on the order-disorder transformation in the subcarbide phase. Finally,

the DTA runs gave the incipient melting temperatures close to the homogeneous range of the subcarbide phase; these temperatures are usually difficult to observe using the Pirani-method because relatively little liquid is formed at the incipient melting temperature.

E. METALLOGRAPHY

For the metallographic studies, the specimens were mounted in a mixture of diallylphthalate-lucite-copper base mounting material. After coarse grinding on silicon carbide paper with grit sizes varying from i20 to 600, the samples were polished on a nylon cloth using a slurry of Linde-B alumina (0.3/1) in a 5% chromic acid solution.

To obtain the desired phase contrasts, alloys with carbon concentrations from 0 to 25 At. % were differentiated by anodizing the specimen in a 10% oxalic acid solution. This treatment produced a brownish-red tarnish on the metal grains, while the subcarbide grains remained essentially unaffected. Samples with carbon contents between 28 and 43 At. % were first anodized in a 10% oxalic acid solution, followed by dip-etching in an aqueous aqua regia-hydrofluoric acid solution [9 parts H_2O -1 part (60% HCl -20% HNO_3 -20% HF)] and then further dip-etching in 20% Murakami's solution.

Alloys from the concentration range of 43 to 48 At. % carbon were either dip-etched in a 20% Murakami's solution or a concentrated acid solution of the above described mixture of HCl , HNO_3 , and HF . For excess graphite containing alloys, no etching was required; i. e., the samples were examined in the as-polished state.

The photomicrographs were made on a Zeiss Ultraphot II metallograph.

F. X-RAY ANALYSIS

Debye-Scherrer powder diffraction patterns, using $Cu-K \alpha$ radiation, were made of all samples after melting point, DTA, and solid state investigations as well as of arc-melted samples.

The exposures were taken in a 57.4 mm camera on a Siemens-Crystalloflex II unit; the Bragg-angles of the diffraction lines were measured on a Siemens-Kirem coincidence scale with micrometer dial (2 mm indicator travel per 0.01 mm translational motion of the measuring slide.)

G. CHEMICAL ANALYSIS

Carbon analyses were performed on the carbide starting materials as well as approximately one-quarter of selected experimental alloy samples. They were analyzed for carbon concentration using the direct combustion method, i.e., the carbon content was determined by measuring the thermal conductivity of the combusted CO_2 - O_2 gas mixture in a Leco carbon analyzer.

The results of the carbon analysis on selected experimental alloy samples showed that the carbon loss was never greater than 2 At.%, and in most cases was less than 1 At. %.

IV. EXPERIMENTAL RESULTS

A. THE TANTALUM-NIOBIUM BINARY SYSTEM

Melting point measurements on nine binary alloys showed a continuous decrease of the solidus temperatures with increasing niobium concentration (Figure 12). The melting in each alloy occurred nearly isothermally, indicating a very narrow liquidus plus solidus two-phase field over the entire concentration range. In the metal binary system, tantalum and niobium are known to form an isomorphous alloy system with the solidus temperatures increasing smoothly with the tantalum concentration; earlier works concerning this system have been summarized by R. P. Elliott⁽²³⁾ and W. B. Pearson⁽²⁴⁾.

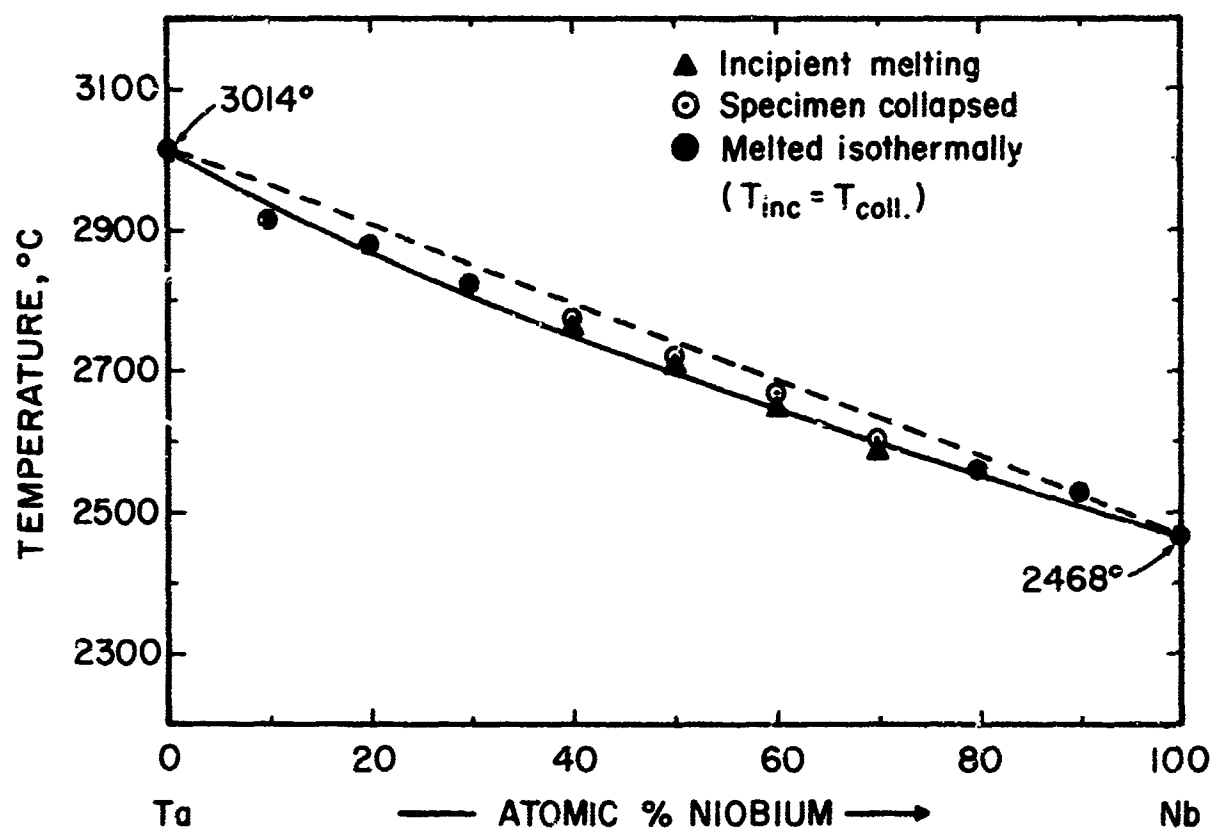


Figure 12. Nb-Ta: Melting Temperatures

B. SOLID STATE PHASE EQUILIBRIA IN THE TERNARY Nb-Ta-C SYSTEM

The phase equilibria of the ternary system niobium-tantalum-carbon, as determined primarily from an X-ray analysis of heat-treated samples at 1800 and 1500°C, are shown in Figures 13 and 14.

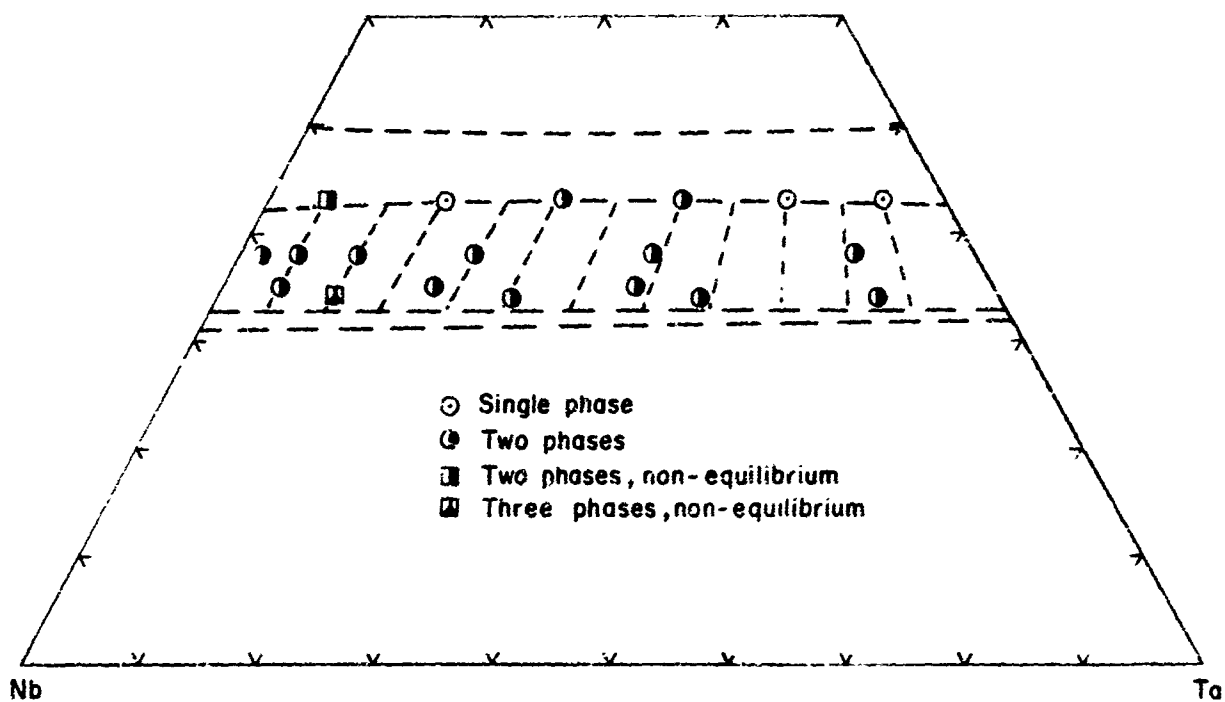


Figure 13. Nb-Ta-C: Qualitative X-ray Evaluation of Alloys Equilibrated at 1800°C

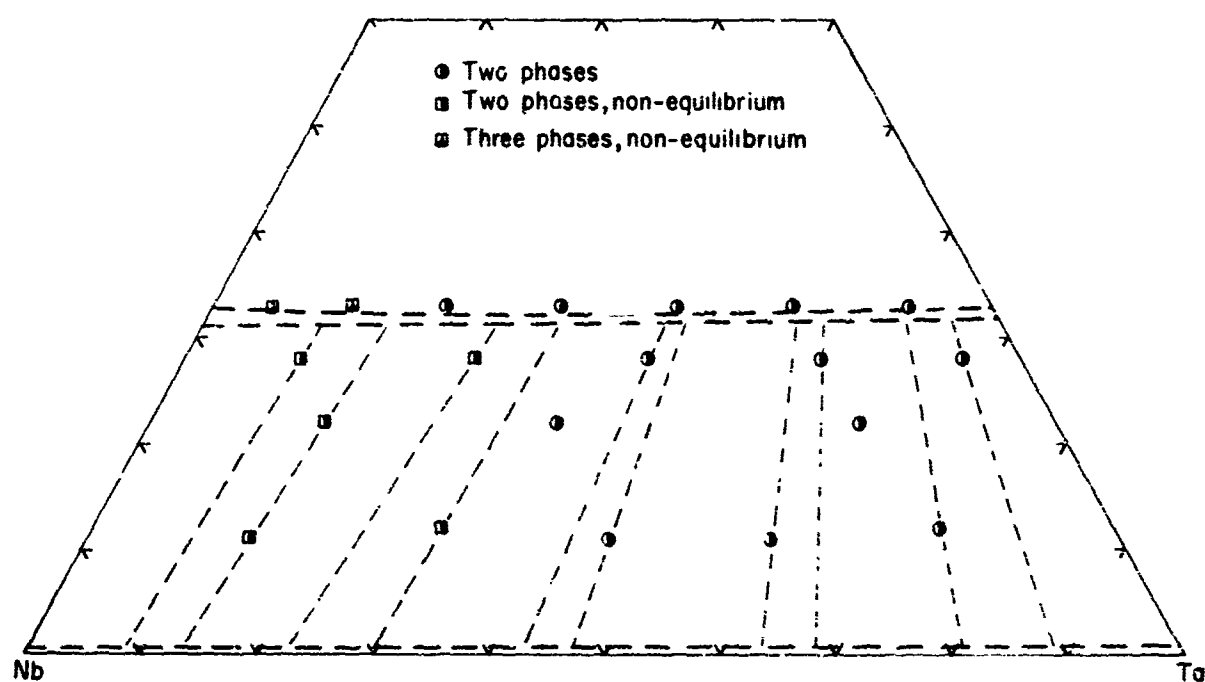


Figure 14. Nb-Ta-C: Qualitative X-ray Evaluation of Alloys Equilibrated at 1500°C

At 1800°C, NbC and TaC form a continuous series of solid solutions as shown by the lattice parameter variations of the cubic monocarbide phase (Figure 15). The lattice parameters of quenched alloys at 38 At. % carbon correspond to compositions in the two-phase field of monocarbide plus subcarbide, while those alloys at 43 At. % carbon are essentially on the lower phase boundary of the monocarbide solid solution.

The variation of the lattice parameters of the hexagonal subcarbide alloys quenched from 1500°C are shown in Figure 16. The lattice parameters of the alloy series at 28 At. % carbon correspond to compositions in the two-phase field of metal plus subcarbide, while the alloy series at 33 At. % carbon varies from ~1 to 2 At. % carbon above the carbon-rich boundary of the subcarbide phase.

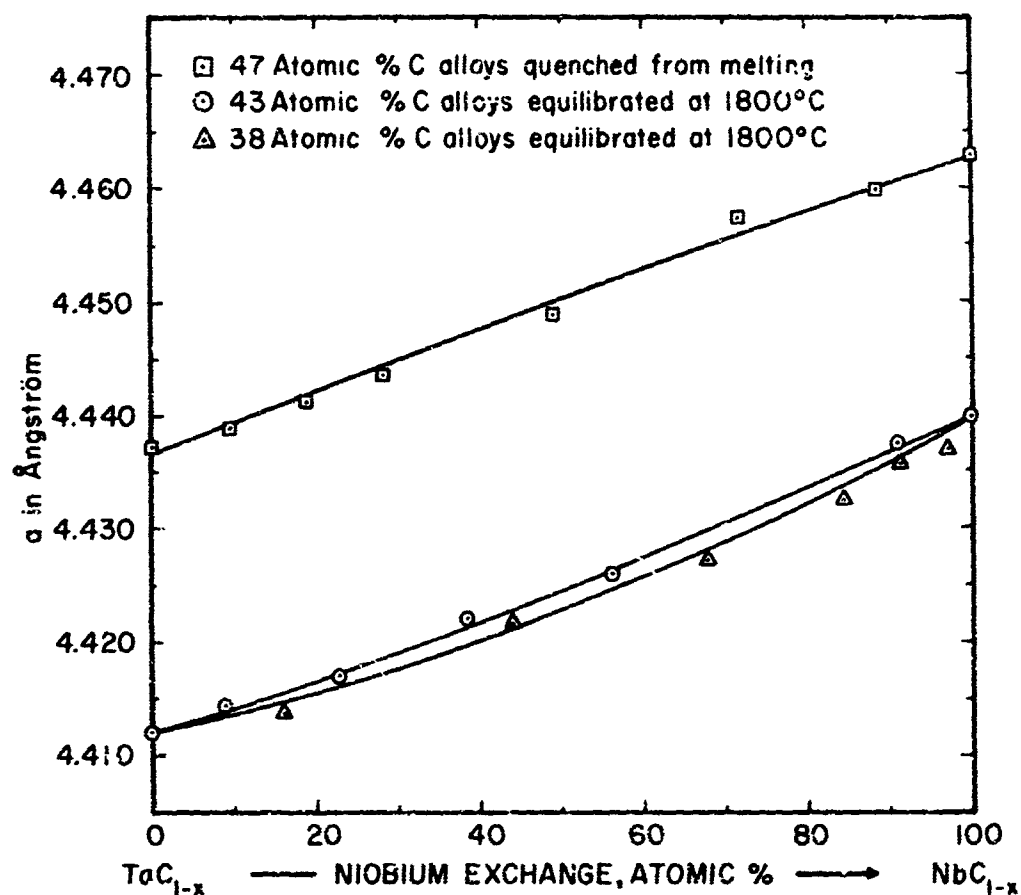


Figure 15. Nb-Ta-C: Lattice Parameters of the Ternary Monocarbide Solid Solution.

The continuous variation of the lattice parameters of the hexagonal subcarbide phase equilibrated at 1500°C would indicate that the low-temperature-ordered modifications of α -Ta₂C and β -Nb₂C form a complete series of solid solutions. But since α -Ta₂C and β -Nb₂C have different ordered structure forms, i. e., the anti-CdI₂ and ϵ -Fe₂N structure types, respectively, there must exist a two-phase field between these two compounds. Therefore, from the X-ray evaluation of alloys equilibrated at both 1500 and 1800°C, the maximum solubilities of Nb₂C in Ta₂C and Ta₂C in Nb₂C could not be determined.

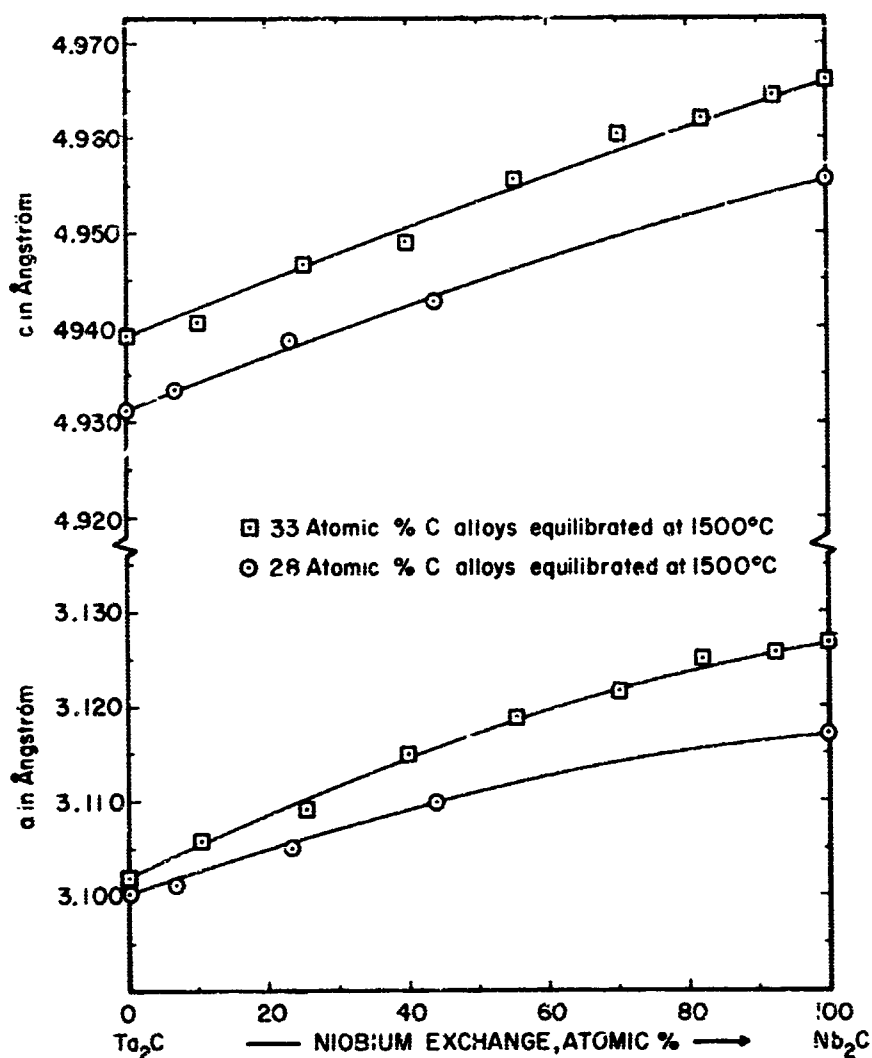


Figure 16. Nb-Ta-C: Lattice Parameters of the Ternary Subcarbide Solid Solutions.

Because the only difference between the two ordered structures of the subcarbide phase lies in the arrangement of the carbon atoms in the metal host lattice, an extensive study by means of neutron and electron diffraction would be required to determine the distribution of the carbon atoms among the interstitial lattice sites; this investigation would reveal the maximum metal exchanges of niobium and tantalum in the two different

(α and β) forms of tantalum and niobium subcarbide, respectively. Therefore, in the present study of this system, the two ordered forms of the subcarbide phase are shown to form a complete series of solid solutions.

As shown in Figures 13 and 14, the tie-line distributions within the metal-subcarbide two phase field at 1500°C and the subcarbide-monocarbide two-phase field at 1800°C were determined by comparing the lattice parameters of the phases present in the two-phased alloys with the lattice parameter variations of the solid solution series. As a result of the lower equilibration temperature of 1500°C, the homogeneity limits of the solid solutions and the compositions of the coexisting phases in the two-phase fields assume slightly different values.

The continuation of the order-disorder phase transformation of Nb_2C and Ta_2C into the ternary is not specifically shown in the section drawings, as was previously mentioned. DTA studies carried out on two alloy series at 28 and 33 At. % carbon revealed the presence of the order-disorder transformation in the subcarbide phase in both hyper- and hypostoichiometric alloys. As shown in the DTA thermograms (cooling) of Figure 17, the order-disorder phase reaction appears quite prominent, but for alloys located farther away from the binary boundary phases the reaction became extremely sluggish both in the metal-rich and carbon-rich subcarbide alloys; and hence the temperature variation of the ordering reaction could not be determined.

Alloys located close to the metal-rich boundary of the subcarbide phase showed a slight decrease in the transition temperatures from ~2480°C for the Nb_2C binary phase and ~2050°C for the Ta_2C binary phase. For the alloys located at approximately the stoichiometric composition of the subcarbide phase, there was also a slight decrease of the transition temperature from ~2500°C for the Nb_2C binary phase and ~2130°C for the Ta_2C binary phase. If this trend in the transformation temperatures continues into the ternary system, the high-temperature-disordered form of $\gamma\text{-(Nb, Ta)}_2\text{C}$ -ss at hyperstoichiometric composition probably participates in either a

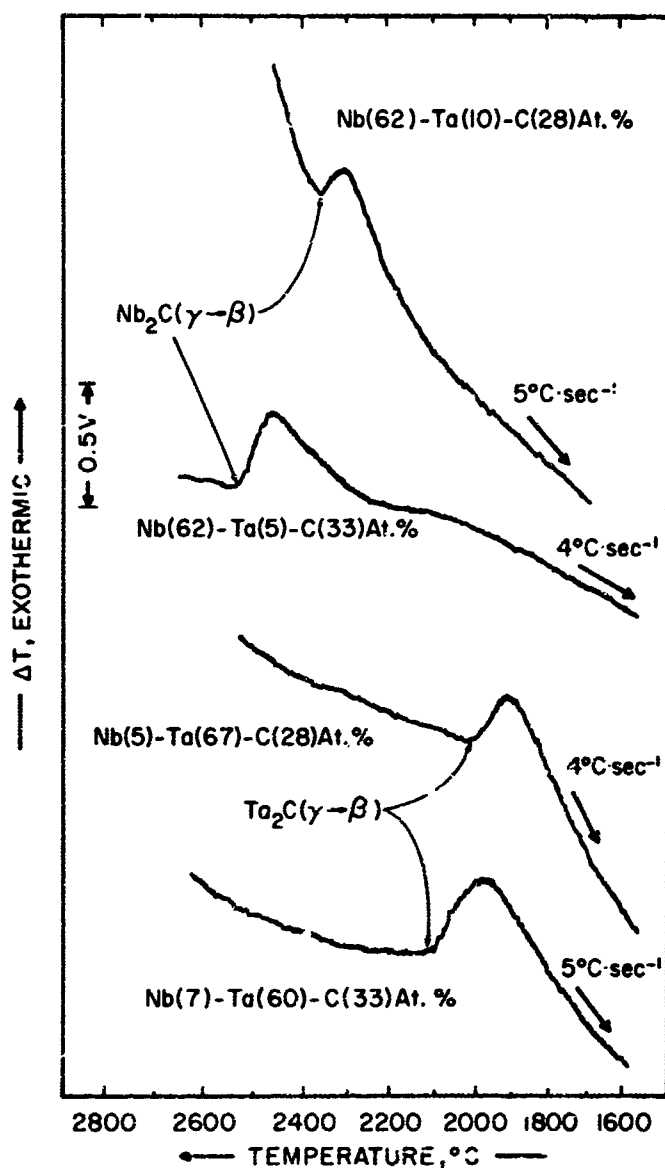


Figure 17. Nb-Ta-C: Order-Disorder Phase Reaction of Nb_2C and Ta_2C in Ternary Alloys: DTA Thermograms (Cooling) of Ternary Alloys Containing 28 and 33 At. % Carbon.

four-phase reaction of the type: $\bar{\gamma}-(\text{Nb}, \text{Ta})_2\text{C}-ss \rightleftharpoons \beta-(\text{Nb}, \text{Ta})_2\text{C}-ss$ (Nb-rich) + $\beta-(\text{Nb}, \text{Ta})_2\text{C}-ss(\text{Ta}, \text{rich}) + \delta-(\text{Nb}, \text{Ta})\text{C}_{1-x}-ss$, or a limiting tie-line reaction of the type $\bar{\gamma}-(\text{Nb}, \text{Ta})\text{C}_{1+x} \rightleftharpoons \beta-(\text{Nb}, \text{Ta})_2\text{C} + \delta-(\text{Nb}, \text{Ta})\text{C}_{1-x}$. The variation of the order-disorder phase reactions as determined from the DTA study is presented in the isopleth at 32.5 At. % C (Figure 5).

The metallographic examination of alloys which participated in the ordering reaction revealed the presence of a substructure in the subcarbide phase (Figures 18 and 19). These mottled areas of the microstructures are associated with the ordering reaction. The proposed reaction sequence which takes place in the subcarbide phase will be discussed in a later section.



Figure 18. Nb-Ta-C: Photomicrograph of a DTA Sample (47-20-33 At. %), Cooled at $\sim 4^{\circ}\text{C}/\text{sec}$ from 2840°C . Monocarbide with Multi-directional Subcarbide Precipitates. Mottled Areas of Microstructure-Transformed Subcarbide (Pores Black). $\times 425$

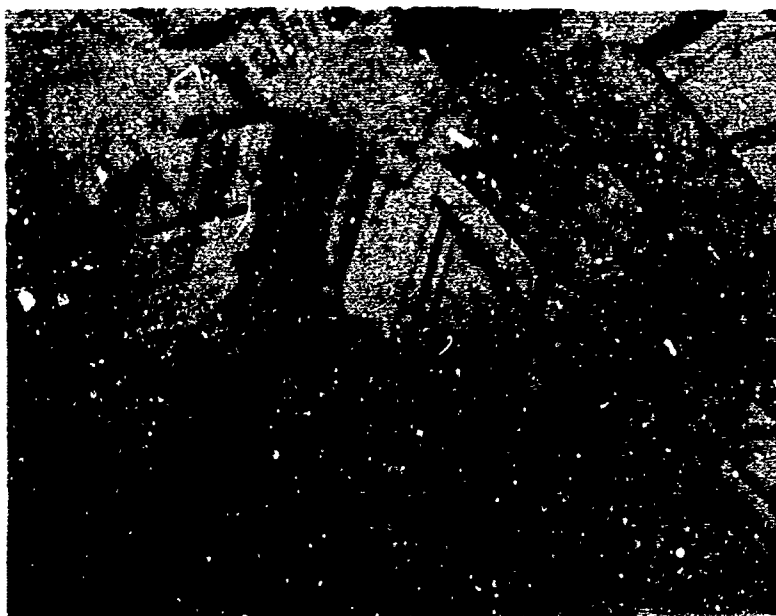


Figure 19. Nb-Ta-C: Photomicrograph of a DTA Sample (55-12-33 At. %), Cooled at $\sim 4^\circ\text{C}/\text{sec}$ from 2740°C . Monocarbide with Multi-directional Subcarbide Precipitates. Mottled Areas of Microstructure-Transformed Subcarbide (Pores Black). $\times 1000$

Because there is no corresponding low-temperature orthorhombic modification of $\alpha\text{-Nb}_2\text{C}$ ($\sim \text{Fe}_2\text{N}$ structure type) in the Ta_2C phase, the effect of tantalum additions on the $\alpha\text{-}\beta\text{-Nb}_2\text{C}$ phase transformation was studied by DTA technique. DTA thermograms of four ternary alloys are presented in Figure 20. The thermal arrests observed on cooling are caused by the stabilization of the orthorhombic modification of $\alpha\text{-Nb}_2\text{C}$ into the ternary system. The temperature of the $\alpha\text{-}\beta\text{-Nb}_2\text{C}$ phase transformation is raised from 1230°C in the Nb-C binary system with the α -phase ultimately being terminated at a maximum temperature of $\sim 1430^\circ\text{C}$ at a tantalum exchange of approximately 34 At. % (Figure 5).

The displacive transformation of the Nb_2C -ss appears to be sluggish at the carbon-rich boundary of the phase as was previously reported by E. Rudy, S. Windisch, and C. E. Brukl⁽⁵⁾, while alloys near the

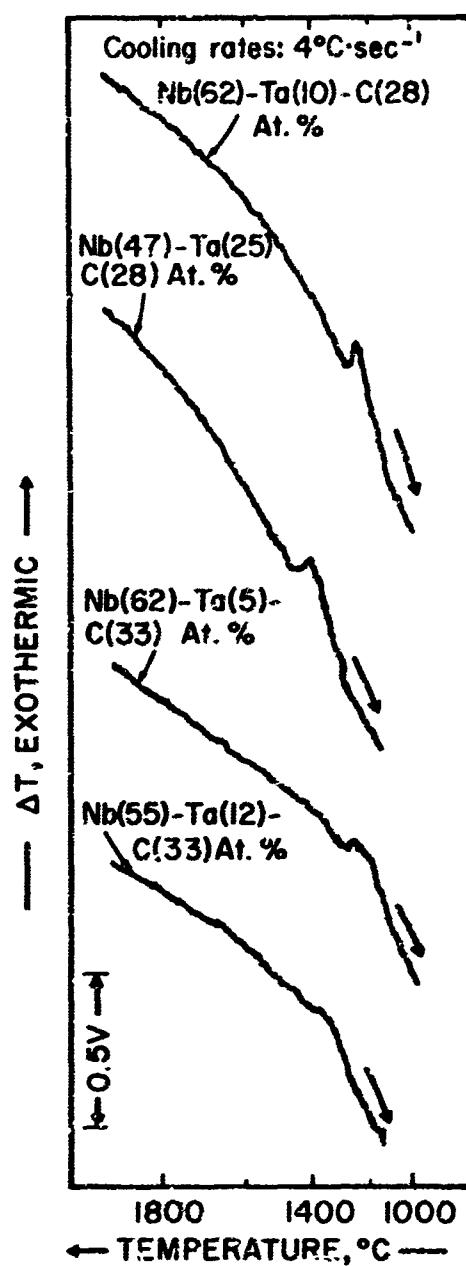


Figure 20. Nb-Ta-C: α - β -Nb₂C Phase Reaction in Ternary Alloys: DTA Thermograms (Cooling) of Alloys Located in the Vicinity of Nb₂C.

metal-rich phase boundary appear to undergo the transformation more rapidly. This is evidenced by comparing the size of the enthalpy changes shown by the two alloy series at 28 and 33 At. % carbon in Figure 20, and also by comparing the microstructures of the heat-treated alloys which were furnace quenched from 1500°C (Figure 14).

The low-temperature α modification is formed by a distortion of the hexagonal β -Nb₂C as reported by E. Rudy and C. E. Brukl⁽⁶⁾. The displacive transformation is recognized by the appearance of slip lines in the subcarbide grains (Figures 21 and 22).

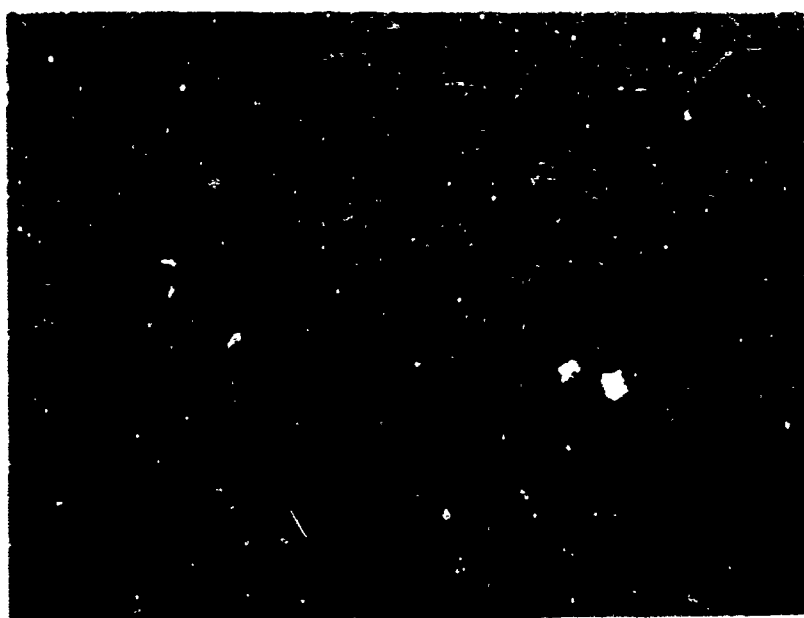


Figure 21. Nb-Ta-C: Photomicrograph of a DTA Sample (55-12-33 At. %), X680 Cooled at $\sim 4^\circ\text{C}/\text{sec}$ from 2740°C and Heat-Treated at 1500°C for 64 hr. Slip Lines in (Nb, Ta)₂C-ss Resulting from the Displacive Transformation $\beta \rightarrow \alpha$. Trace of Monocarbide Precipitates within Subcarbide Grains (Pores Black).

From the X-ray analysis of the DTA alloys at 28 and 33 At. % carbon, those alloys which participated in the displacive transformation exhibited only two phases in equilibrium. That is, in alloys cooled from $\sim 2700^\circ\text{C}$ at $4^\circ\text{C}/\text{sec}$ and, for example, at a composition of 47Nb-25Ta-28C, At. %, two phases exist in equilibrium -- (Nb, Ta)-ss + (Nb, Ta)₂C-ss

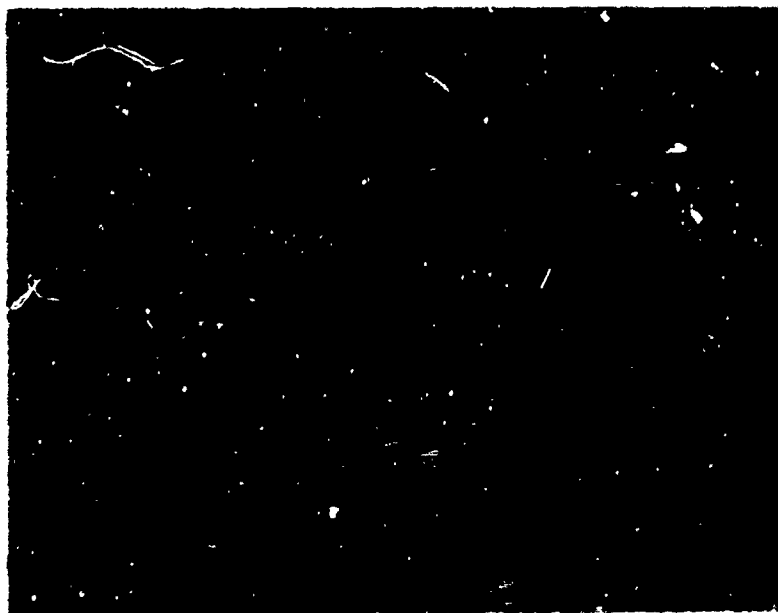


Figure 22. Nb-Ta-C: Photomicrograph of a DTA Sample (62-5-33 At. %), X1000 Cooled at $\sim 4^\circ\text{C}/\text{sec}$ from 2730°C and Heat-Treated at 1500°C for 64 hr. Slip Lines in (Nb, Ta) C-ss Resulting from the Displacive Transformation of $\beta \rightarrow \alpha$. Trace of Monocarbide Precipitates within Subcarbide Grains.

($a = 12.32_2 \text{ \AA}$, $b = 10.86_3 \text{ \AA}$, $c = 4.74_2 \text{ \AA}$); at a composition of 55Nb-12Ta-33C At. % -- (Nb, Ta) C_{1-x} -ss + (Nb, Ta) C_{2-x} -ss ($a = 12.36_5 \text{ \AA}$, $b = 10.88_8 \text{ \AA}$, $c = 4.96_0 \text{ \AA}$). Therefore, the displacive transformation in both the hypo- and hyperstoichiometric phase, when cooling conditions are sufficiently slow, is probably single phased and not of the first order.

C. PHASE EQUILIBRIA AT HIGH TEMPERATURES

The location of the maximum solubility curve of carbon in niobium-tantalum alloys, of the metal-rich eutectic trough, and of the metal-rich phase boundary of the subcarbide phase, was established by the metallographic examination of alloys having carbon concentrations between 2 and 28 At. %.

The solid solubility of carbon in both niobium and tantalum is strongly temperature-dependent as shown by Figures 7 and 8. The maximum

solubility of carbon in both these metals is 7.5 At. % at temperatures of 2353°C (Nb + Nb₂C eutectic) and 2843°C (Ta + Ta₂C eutectic). In three ternary alloy series with carbon concentrations of 2, 5, and 8 At. %, which were arc-melted, the metallographic examination showed the same type of precipitation structures which were found in the metal-carbon binary systems^(5, 12). The microstructures of rapidly quenched arc-melted alloys exhibited an essentially random distribution of the (Nb, Ta)₂C precipitates in the (Nb, Ta) matrix, and also a tendency for the subcarbide phase to segregate to the grain boundaries of the metal phase (Figures 23, 24, and 25). The ternary alloy at 5 At. % C (Figure 24) shows a slight trace of the (Nb, Ta) + (Nb, Ta)₂C eutectic in the metal grain boundaries.

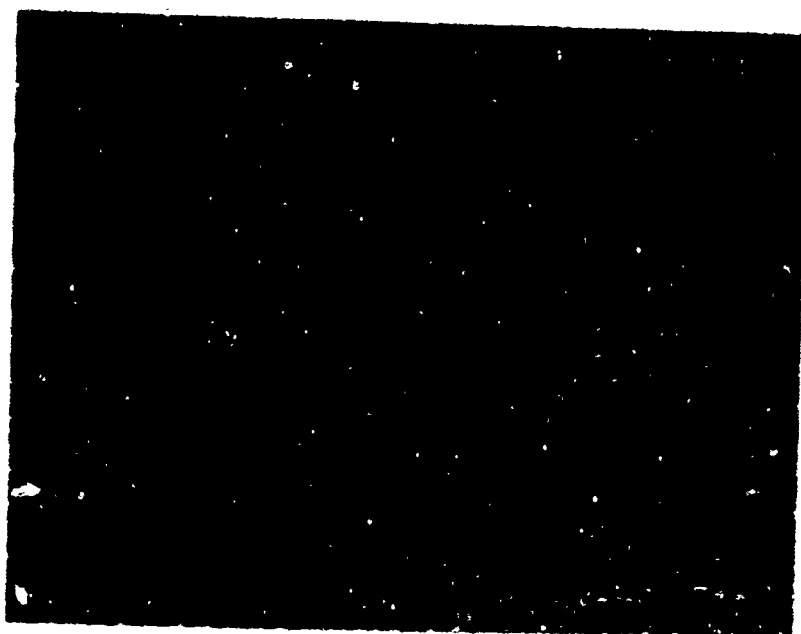


Figure 23. Nb-Ta-C: Photomicrograph of an Arc-Melted Sample (49-49-2 At. %). Primary (Nb, Ta) Grains with Intra-granular (Nb, Ta)₂C Precipitations. Note Segregation of Precipitate Phase to the Grain Boundaries.

X220



Figure 24. Nb-Ta-C: Photomicrograph of an Arc-Melted Sample (48-47-5 At. %). Primary (Nb, Ta) Grains with Intragranular $(\text{Nb, Ta})_2\text{C}$ Precipitations. Trace of $(\text{Nb, Ta}) + (\text{Nb, Ta})_2\text{C}$ Eutectic Plus Segregated $(\text{Nb, Ta})_2\text{C}$ Precipitates in the Grain Boundaries.

X270

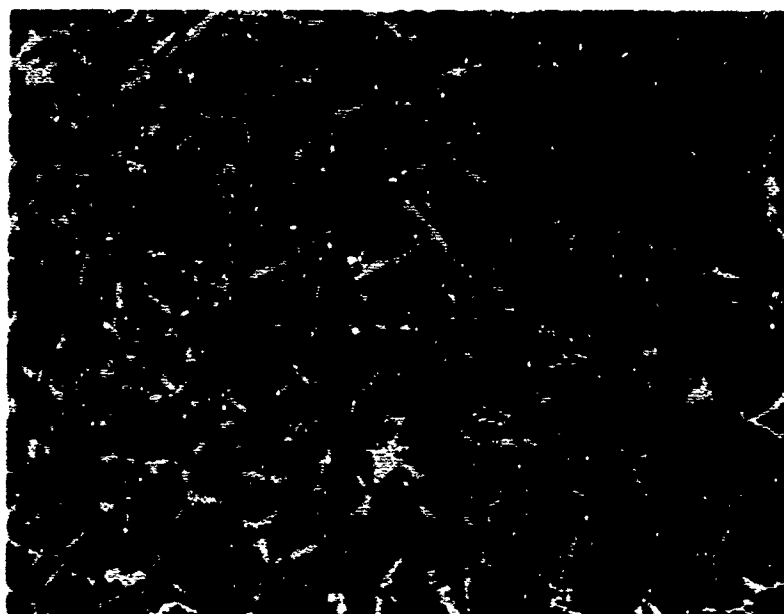


Figure 25. Nb-Ta-C: Photomicrograph of an Arc-Melted Sample (46-46-8 At. %). Primary (Nb, Ta) Grains with Intragranular $(\text{Nb, Ta})_2\text{C}$ Precipitations. $(\text{Nb, Ta}) + (\text{Nb, Ta})_2\text{C}$ Eutectic Plus Segregated $(\text{Nb, Ta})_2\text{C}$ Precipitates in the Grain Boundaries.

X210

The eutectic trough, extending from the Nb + Nb₂C eutectic isotherm at 2353°C and 10.5 At.% C to the Ta + Ta₂C eutectic isotherm at 2643°C and 12 At.% C, is shown in Figure 26. The location of this curve was determined from the metallographic examination of both arc-melted and melting point alloys at 11 and 12 At.% C in conjunction with the tie-line distribution in this region. All alloys located at or close to the eutectic trough melted fairly isothermally; this indicated that the three-phase boundaries must be extremely narrow, i.e., only a small gap exists between the solidus and liquidus temperatures. This behavior is also reflected in the microstructures, which closely resemble the metal-matrix type eutectic structures found in the two metal-carbon binary systems of niobium and tantalum^(5, 12). The microstructures of these ternary alloys which underwent bivariant eutectic solidification are shown in Figures 27, 28, and 29.

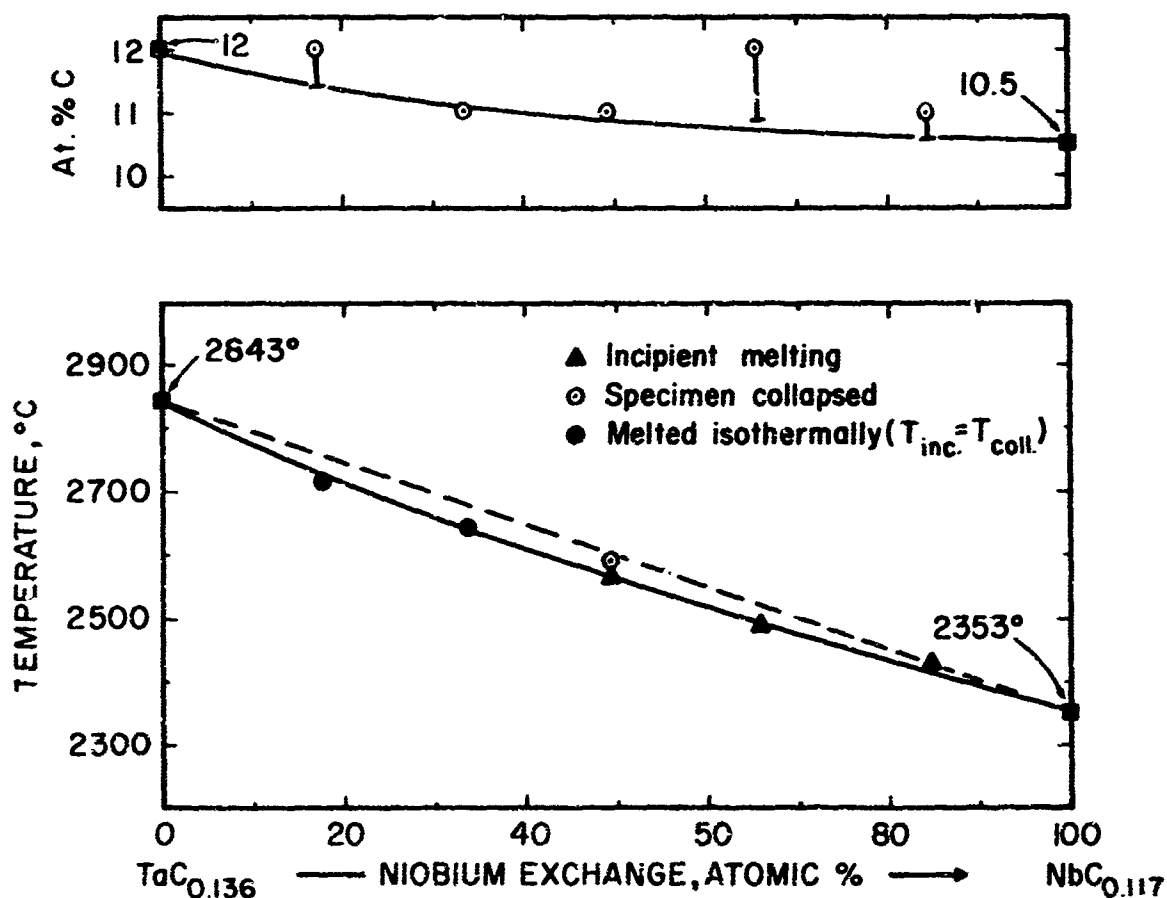


Figure 26. Nb-Ta-C: Melting Temperatures (Bottom) and Location (Top) of the Metal-Rich Eutectic Trough Between (Nb, Ta) and (Nb, Ta)₂C.

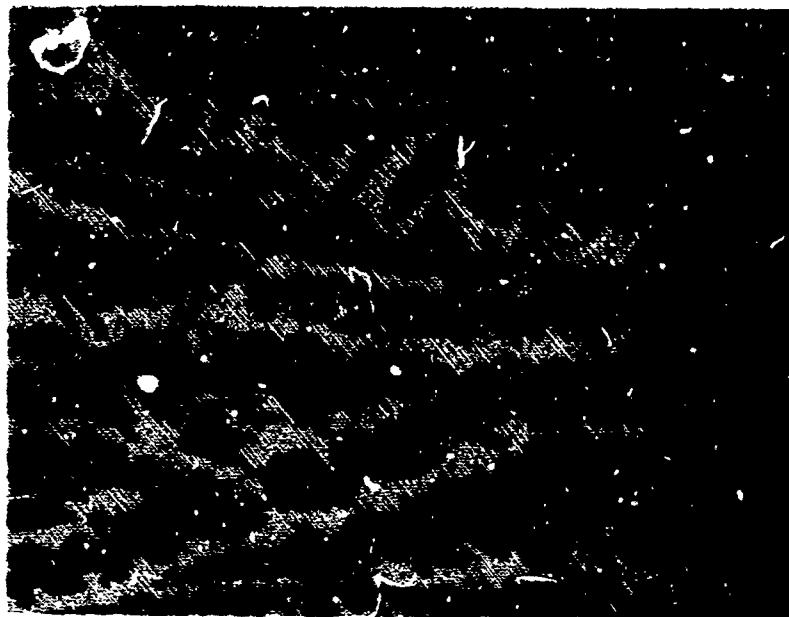


Figure 27. Nb-Ta-C: Photomicrograph of an Arc-Melted Sample (75-14-11 At. %). Traces of Primary $(\text{Nb, Ta})_2\text{C}$ in a $(\text{Nb, Ta}) + (\text{Nb, Ta})_2\text{C}$ Eutectic Matrix.

X520



Figure 28. Nb-Ta-C: Photomicrograph of an Arc-Melted Sample (30-59-11 At. %). $(\text{Nb, Ta}) + (\text{Nb, Ta})_2\text{C}$ Eutectic.

X400

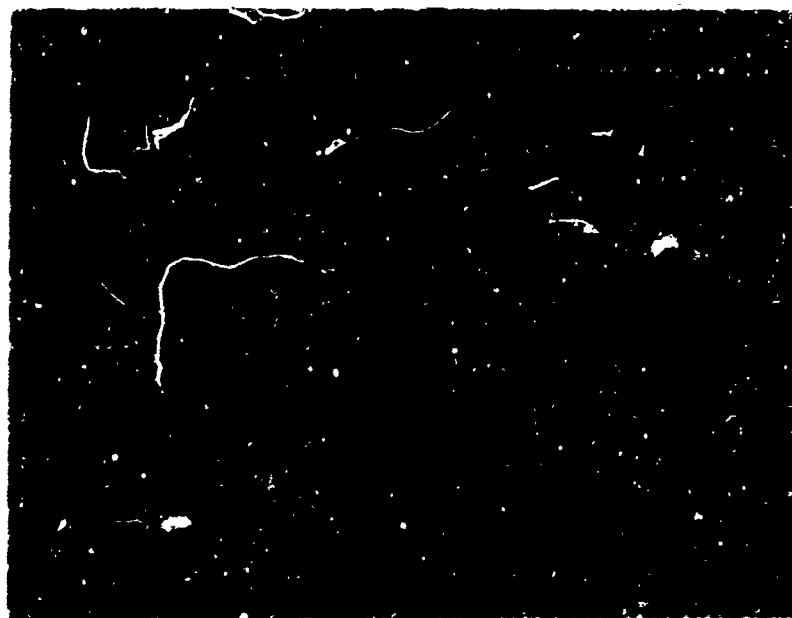


Figure 29. Nb-Ta-C: Photomicrograph of an Arc-Melted Sample (15-73-12 At.%). Slight Trace of Primary $(\text{Nb, Ta})_2\text{C}$ in $(\text{Nb, Ta}) + (\text{Nb, Ta})_2\text{C}$ Eutectic Matrix. X200

Typical microstructures of alloys located in the vicinity of the metal-rich homogeneity limits of the $(\text{Nb, Ta})_2\text{C}$ phase at the (Nb, Ta) - $(\text{Nb, Ta})_2\text{C}$ eutectic temperatures are shown in Figures 30 and 31. These photomicrographs show the primary $(\text{Nb, Ta})_2\text{C}$ grains with intragranular metal precipitations and varying amounts of (Nb, Ta) at the grain boundaries (subcarbide depleted eutectic).

The ternary subcarbide solid solution $(\text{Nb, Ta})_2\text{C}$ melts peritectically in a manner similar to the binary phases, Nb_2C and Ta_2C . The variation of the peritectic temperatures was determined by measuring the incipient melting points of 14 alloys having carbon concentrations between 25 and 35 At. %.

Figure 32 shows the melting behavior of alloys which participated in the peritectic melting of the subcarbide phase. The majority of the alloys melted very heterogeneously, especially those at 30 and 35 At. %C.

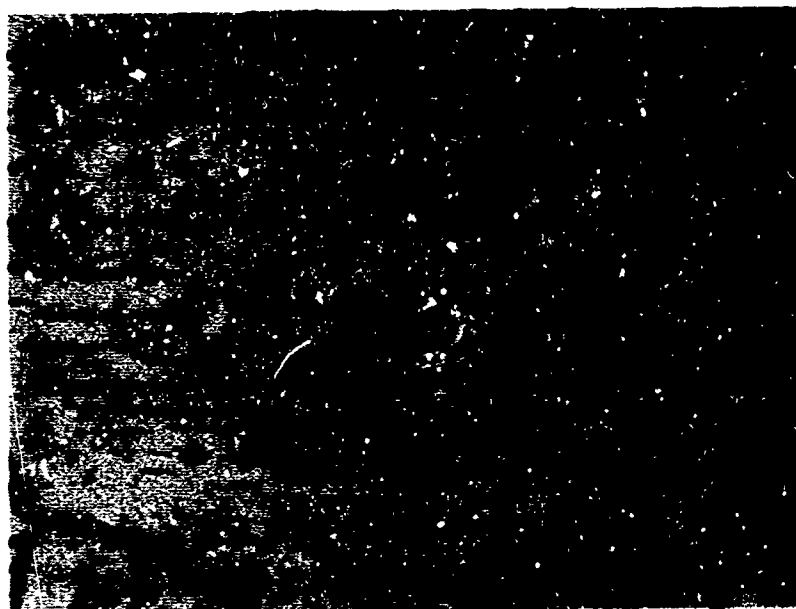


Figure 30. Nb-Ta-C: Photomicrograph of a DTA Sample (62-10-28 At.%), Cooled at $\sim 3^\circ\text{C}/\text{sec}$ from 2770°C . Primary Nb-Rich $(\text{Nb}, \text{Ta})_2\text{C}$ with Intragranular Metal Precipitations. Small Amounts of Metal Phase at the Grain Boundaries.

X475



Figure 31. Nb-Ta-C: Photomicrograph of a DTA Sample (32-40-28 At.%), Quenched from 2750°C . Primary $(\text{Nb}, \text{Ta})_2\text{C}$ with Intragranular Metal Precipitations in a SiC-carbide Depleted-Metal Eutectic Matrix (Pores Black).

X1000

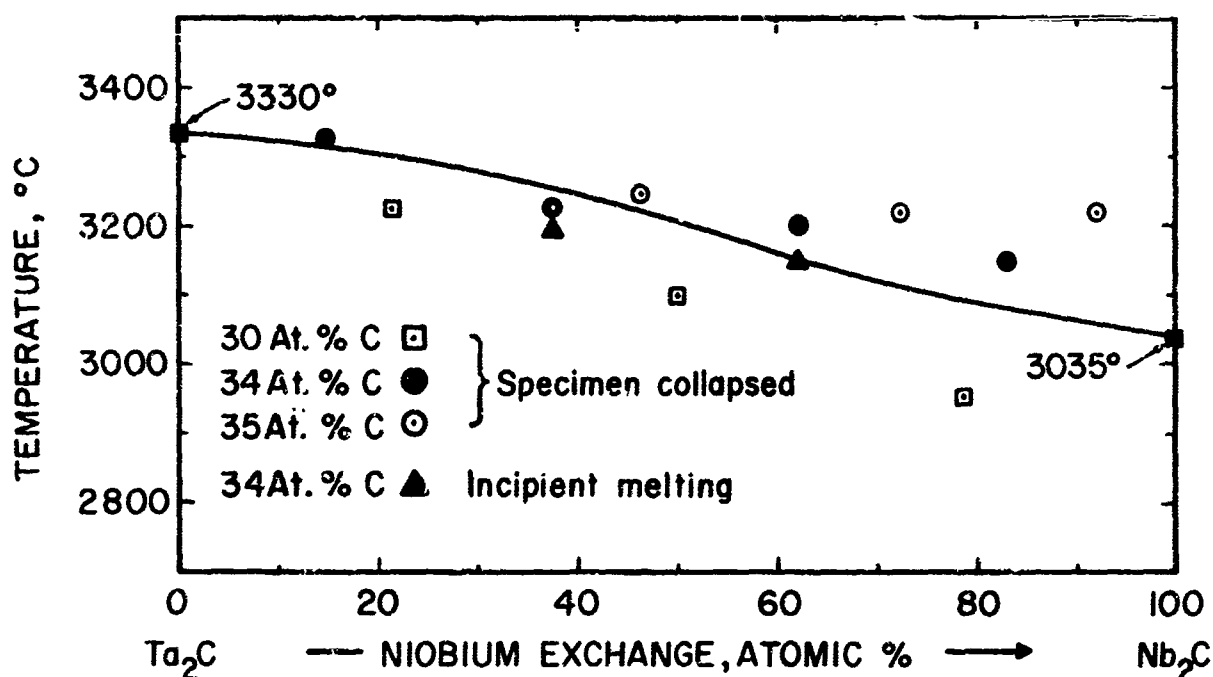


Figure 32. Nb-Ta-C: Peritectic Melting Temperatures of the Solid Solution - $(\text{Nb, Ta})_2\text{C}$.

This extreme two-phase melting results from the steep solidus surfaces of the subcarbide and monocarbide phases; therefore, the collapsing temperatures of these alloys along with their metallographic examination were used to determine the maximum melting and location of the $(\text{Nb, Ta})_2\text{C}$ -ss boundary.

A photomicrograph showing the peritectic-type reaction is presented in Figure 33. This structure shows the peritectic-like nonequilibrium mixture of metal, subcarbide, and monocarbide. The microstructures of ternary alloys located closer to the Ta-C binary system did not yield nonequilibrium structures like that shown in Figure 33. For example, in alloys which were equilibrated above the solidus temperatures, the peritectic reaction did not proceed to completion during rapid cooling. A typical microstructure is presented in Figure 34, which shows the nonequilibrium structure consisting of metal, subcarbide, and monocarbide. Also, the unidirectional monocarbide precipitations in the $(\text{Nb, Ta})_2\text{C}$ grains give evidence for the extension of the carbon-rich phase boundary to hyperstoichiometric composition in ternary subcarbide alloys.



Figure 33. Nb-Ta-C: Photomicrograph of a Melting Point Sample (60-5-35 At. %), Quenched from $\sim 3200^{\circ}\text{C}$.

X680

Non-equilibrium Mixture Resulting from the Peritectic-Type Four-Phase Reaction: $\text{L} + (\text{Nb, Ta})\text{C}_{1-x} \rightarrow (\text{Nb, Ta})_2\text{C} + (\text{Nb, Ta})$.

Center of Grains: $(\text{Nb, Ta})\text{C}_{1-x}$ with $(\text{Nb, Ta})_2\text{C}$ Precipitations.

Light Region: $(\text{Nb, Ta})_2\text{C}$

Matrix: Eutectic $(\text{Nb, Ta}) + (\text{Nb, Ta})_2\text{C}$

The maximum solidus temperatures of the monocarbide solid solution decrease rapidly from the congruent melting point of tantalum monocarbide at 3985 to $\sim 3750^{\circ}\text{C}$; then the melting temperatures decrease gradually to 3613°C , the congruent melting point of niobium monocarbide (Figure 35). Both the melting point variation and location of the maximum solidus temperature between the two binary phases (TaC and NbC) were determined from over 20 melting point measurements covering the solidus envelope of the ternary monocarbide solid solution.

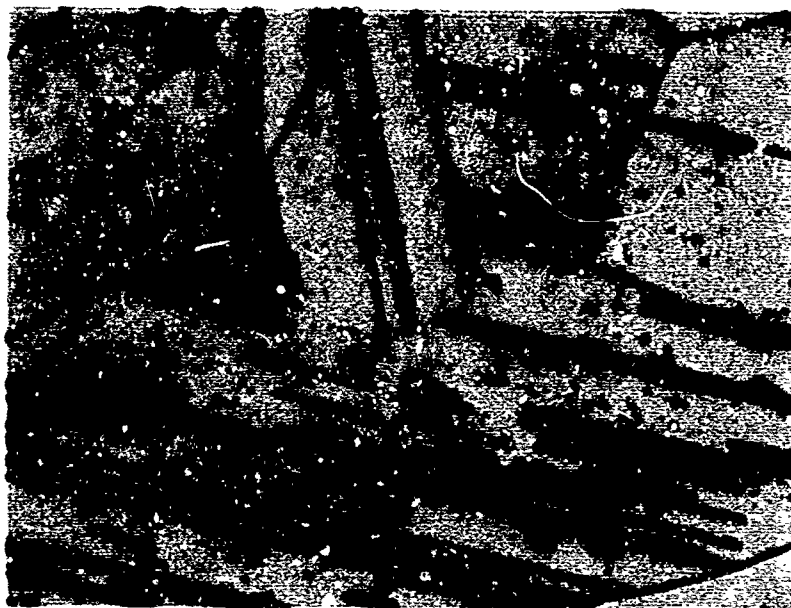


Figure 34. Nb-Ta-C: Photomicrograph of a Melting Point Sample (47-18-35 At. %), Quenched from 3200°C and Equilibrated at 2700°C. X625

Unidirectional $(Nb, Ta)C_{1-x}$ Precipitations in $(Nb, Ta)_2C$ Grains Plus Trace of Metal.

With the exception of alloys located close to the maximum solidus temperature of the monocarbide solid solution between ~20 At. % Nb exchange and the binary phase NbC, the melting of the ternary monocarbide solid solution was extremely heterogeneous.

The melting temperatures of alloys located on either side of the maximum solidus drop rapidly to lower values. Because of the rapid decrease of the maximum solidus temperatures of the monocarbide solid solution into the ternary from the congruent melting tantalum monocarbide, the differences between the liquidus and solidus temperatures become large; but as the slope of the solidus becomes less, the liquidus begins to converge on the solidus until they meet at the congruent melting niobium monocarbide.

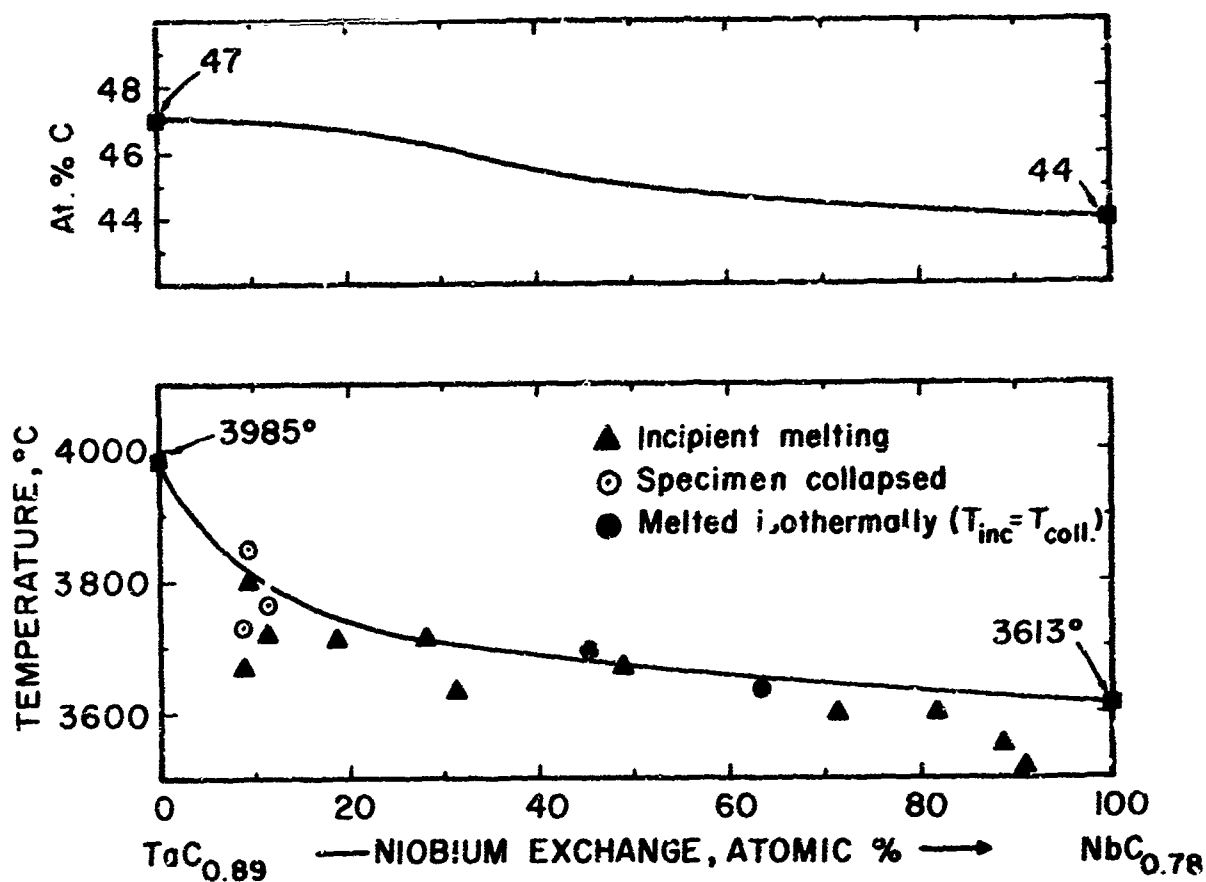


Figure 35. Nb-Ta-C: Maximum Solidus Temperatures of the Ternary Monocarbide Phase.

Top: Concentration Line of the Maximum Solidus.

As a result of this, alloys quenched from liquidus temperatures above the maximum solidus exhibited various degrees of coring as a function of the niobium exchange (Figures 36, 37, and 38).

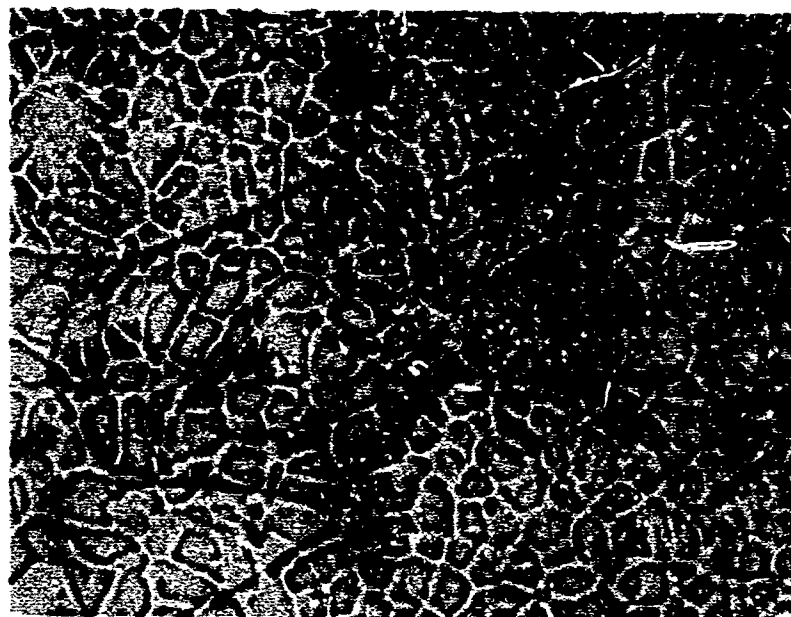


Figure 36. Nb-Ta-C: Photomicrograph of a Melting Point Sample (10-43-47 At. %), Quenched from 3700°C. Cored Monocarbide Solid Solution.

X300

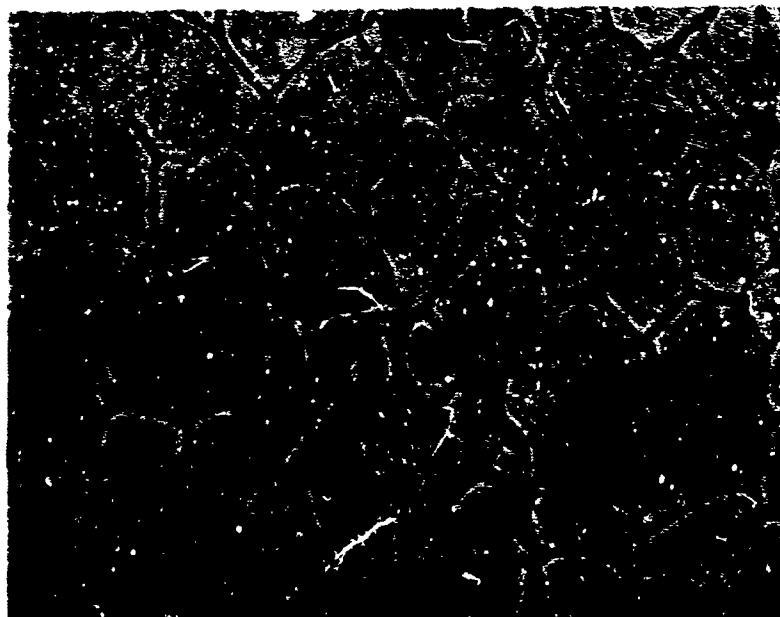


Figure 37. Nb-Ta-C: Photomicrograph of a Melting Point Sample (25-30-45 At. %), Quenched from 3700°C. Cored Monocarbide Solid Solution.

X320

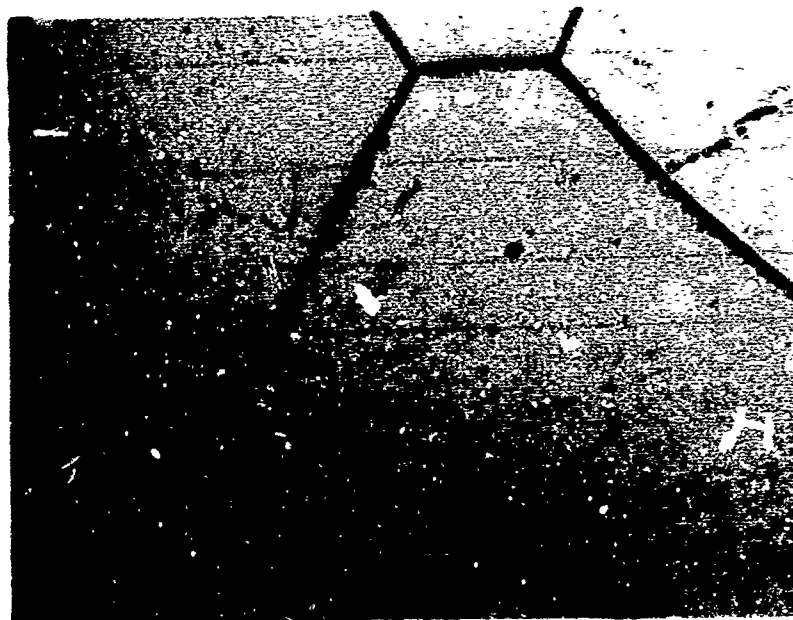


Figure 38. Nb-Ta-C: Photomicrograph of a Melting Point Sample (40-15-45 At. %), Quenched from 3550°C. Single-Phase Monocarbide Solid Solution. X800

The temperature variation and location of the carbon-rich eutectic rough between the monocarbide solid solution and graphite are presented in Figure 39. Alloys in the composition area of monocarbide + graphite exhibited slightly heterogeneous melting, and this indicated that only a small gap existed between the solidus and liquidus temperatures. As a result, even though these ternary alloys underwent bivariant eutectic solidification, eutectic-like structures similar to those found in the respective binaries were also present in the ternary alloys (Figures 40 and 41).

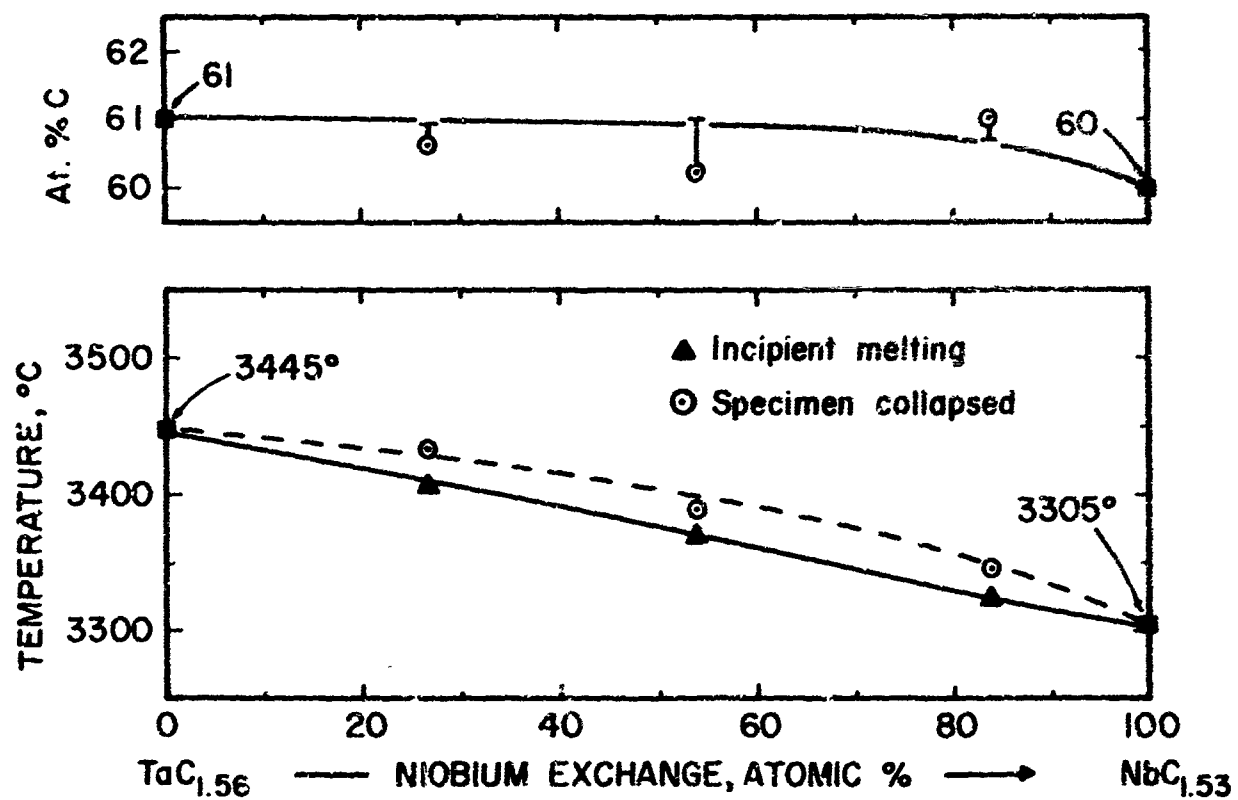


Figure 39. Nb-Ta-C: Experimental Solidus Temperatures and Location of the Eutectic Trough Between the Monocarbide Solid Solution and Graphite.



Figure 40. Nb-Ta-C: Photomicrograph of a Melting Point Sample (11-28-61 At. %), Quenched from 3430°C. Primary Monocarbide Plus (Nb, Ta)C + C Eutectic.

X150



Figure 41. Nb-Ta-C: Photomicrograph of a Melting Point Sample (33-6-61 At. %), Quenched from 3350°C. (Nb, Ta)C + C Eutectic. Very Slight Trace of Primary Graphite.

X150

All melting point data for the two binary systems of Nb-C and Ta-C shown in the preceding figures were obtained from previous works^(5, 12) published at this laboratory.

D. ASSEMBLY OF THE PHASE DIAGRAM

The experimental investigation of the solid state sections in conjunction with the results obtained from melting point, DTA, and metallographic studies were used to construct the isothermal sections covering the range from 1500 to 3806°C (Figures 42 through 53). Finally, the melting point data obtained on ternary alloys were used to construct the liquidus projections shown in Figure 54. These projections are consistent with both the binary systems and the isothermal sections.

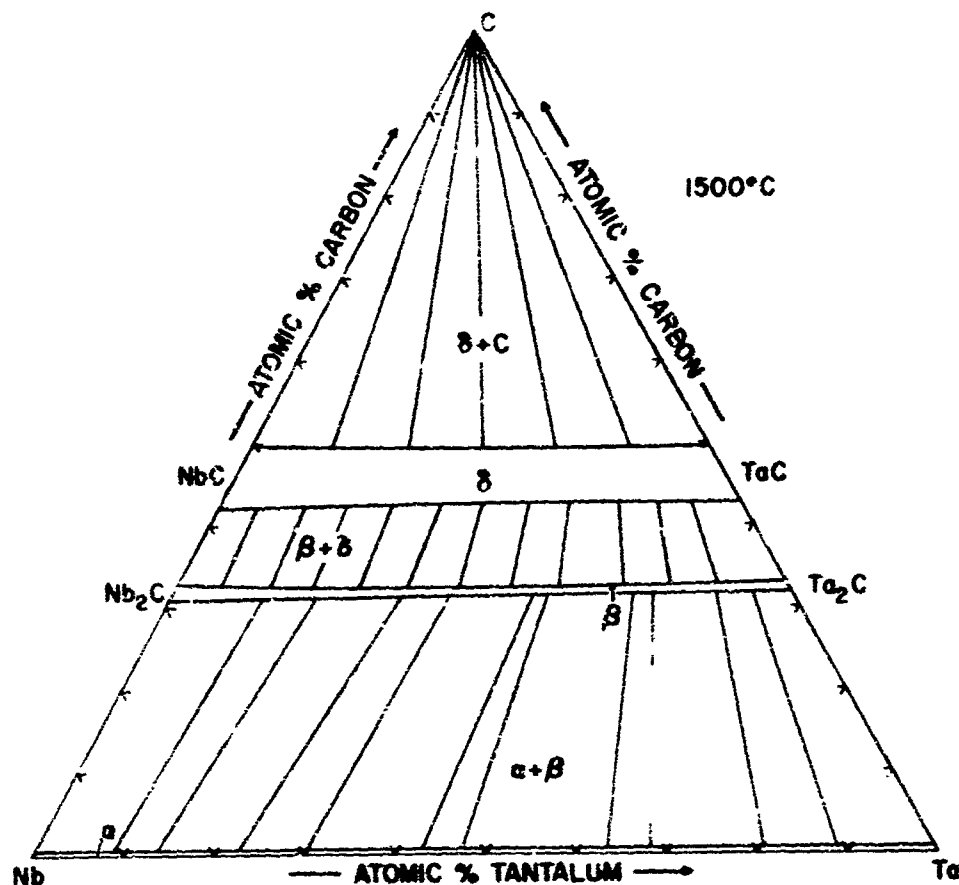


Figure 42. Nb-Ta-C: Isothermal Section at 1500°C

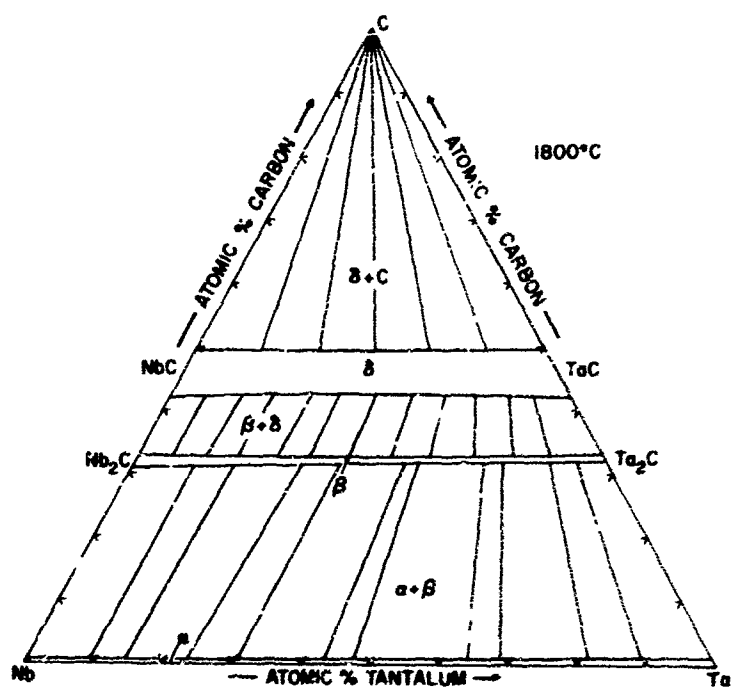


Figure 43. Nb-Ta-C: Isothermal Section at 1800°C

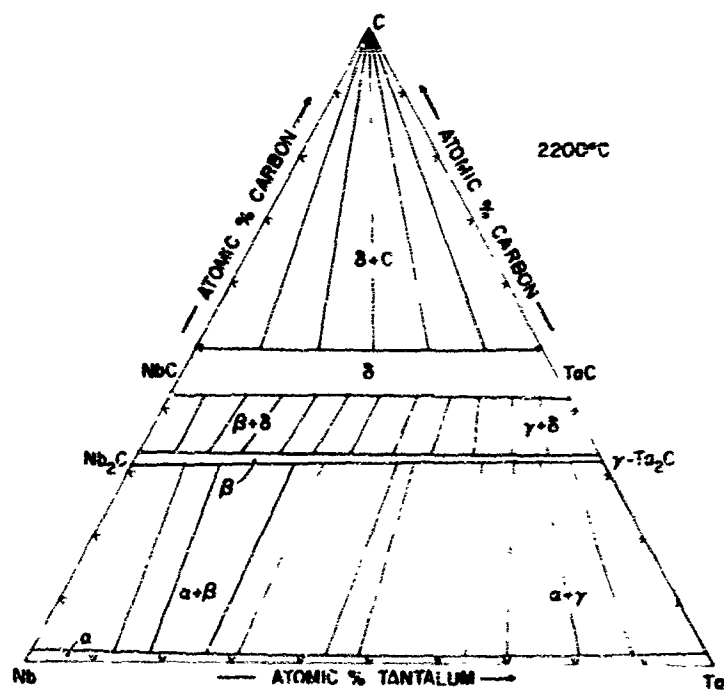


Figure 44. Nb-Ta-C: Isothermal Section at 2200°C

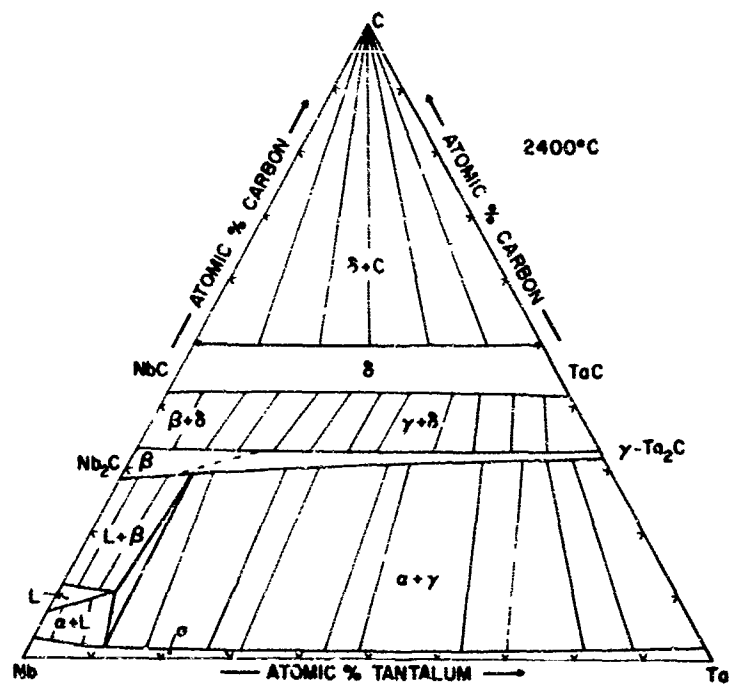


Figure 45. Nb-Ta-C: Isothermal Section at 2400°C

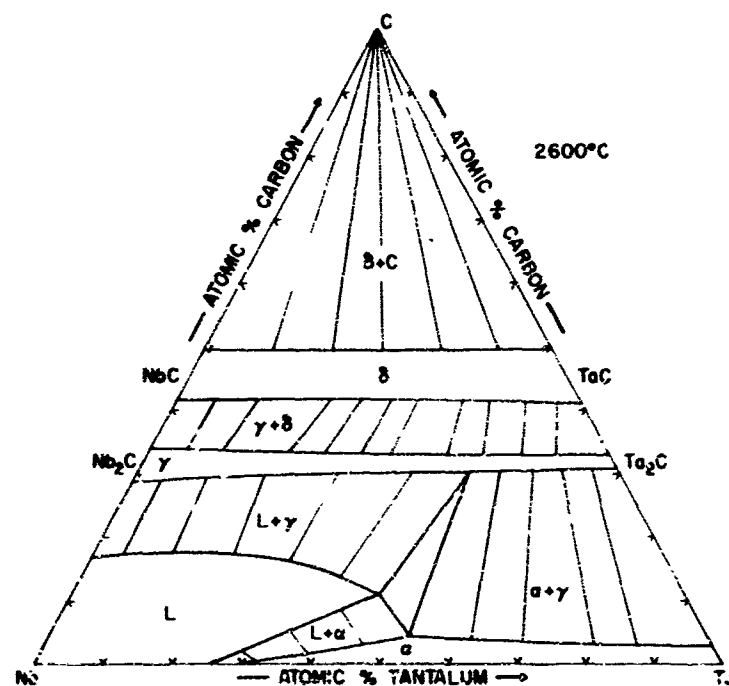


Figure 46. Nb-Ta-C: Isothermal Section at 2600°C

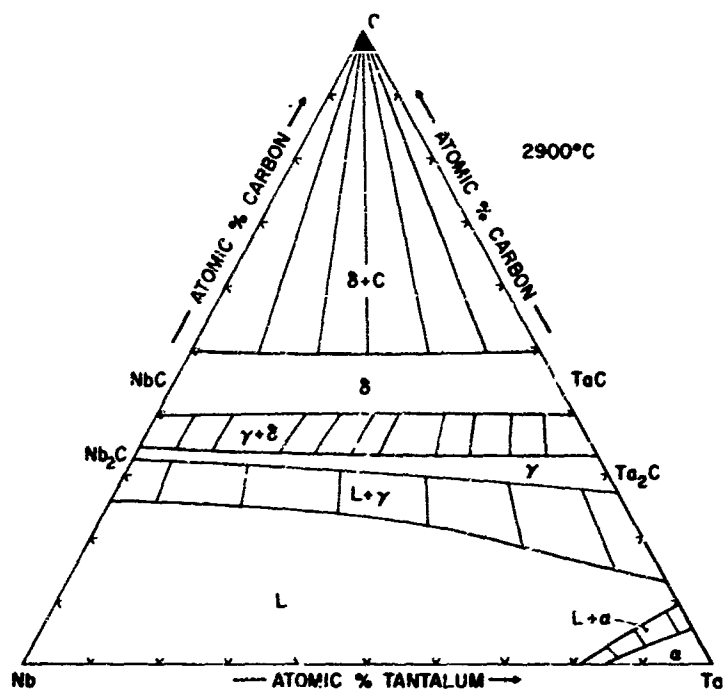


Figure 47. Nb-Ta-C: Isothermal Section at 2900°C

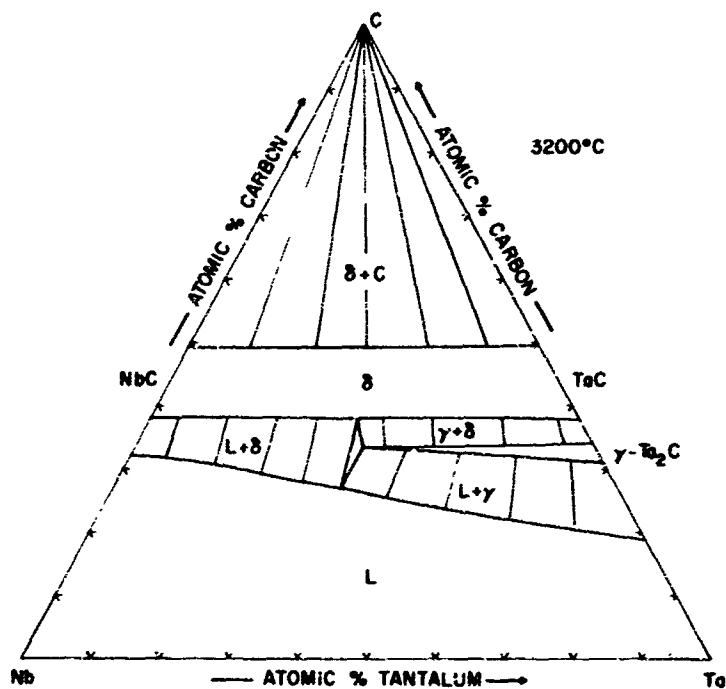


Figure 48. Nb-Ta-C: Isothermal Section at 3200°C

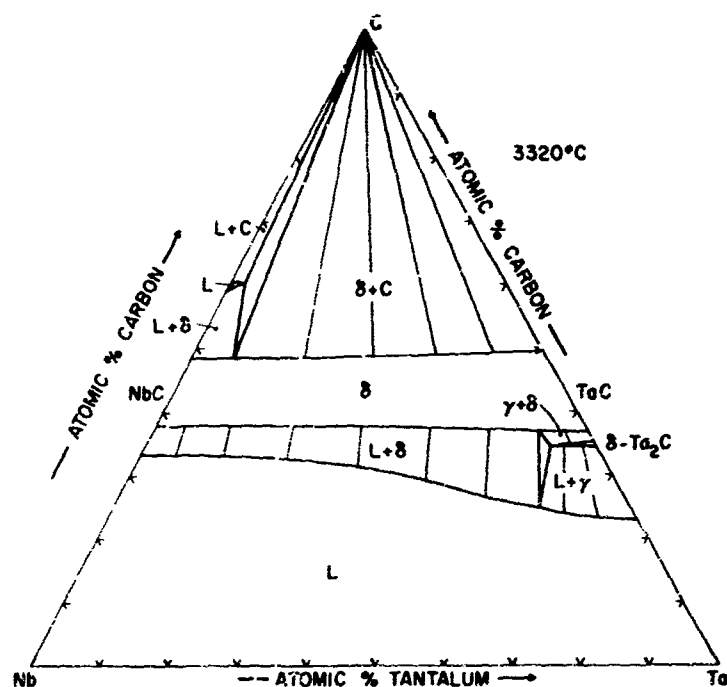


Figure 49. Nb-Ta-C: Isothermal Section at 3320°C

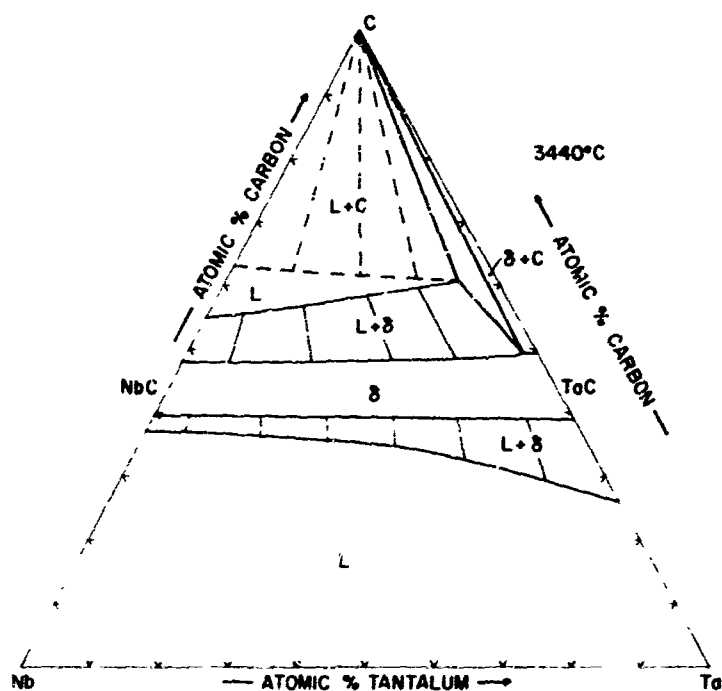


Figure 50. Nb-Ta-C: Isothermal Section at 3440°C

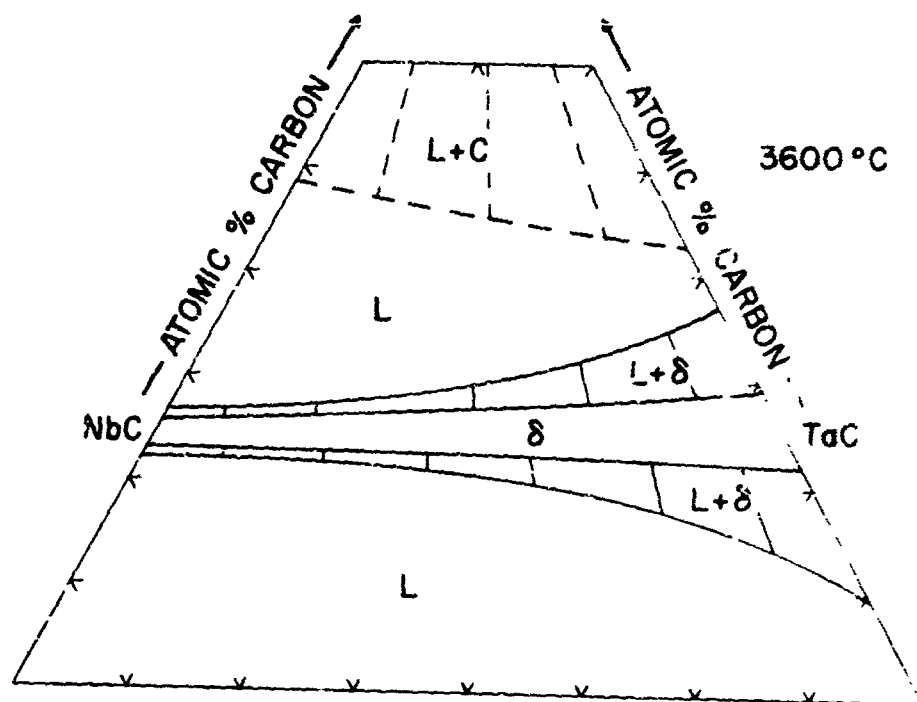


Figure 51. Nb-Ta-C: Isothermal Section at 3600°C

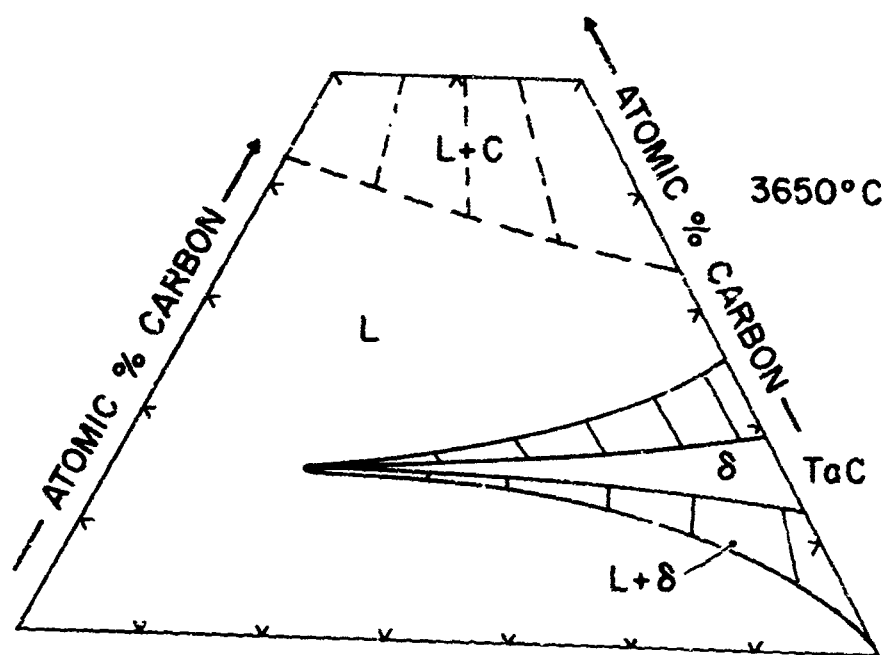


Figure 52. Nb-Ta-C: Isothermal Section at 3650°C

V. CONCLUSIONS AND DISCUSSION

As mentioned previously, the order-disorder phase reaction which occurs in the subcarbide solid solution is not shown in either the section drawings or the isometric view of the entire phase diagram. The DTA study showed the ordering reaction to decrease in temperature into the ternary from the respective binary phases, but the reaction became extremely sluggish in the ternary system, and its temperature variation as a function of metal exchange could not be established. The metallographic examination of alloys located close to the binary phases and also those in the ternary showed identical structures which are associated with the ordering reaction in the subcarbide solid solution.

Therefore, since the order-disorder transition temperatures in Nb_2C and Ta_2C are lowered by the mutual metal exchanges, and assuming that a miscibility gap does not exist between the two ordered forms of the Me_2C -ss; the disordered subcarbide phase will first appear in the ternary system at a limiting tie-line type reaction of the form disordered- $(\text{Nb}, \text{Ta})_2\text{C}_{1+\frac{\text{C}}{\text{X}}}$ ordered- $(\text{Nb}, \text{Ta})_2\text{C} + (\text{Nb}, \text{Ta})\text{C}_{1-\text{X}}$. The proposed reaction sequence for the initiation of the disordered subcarbide phase is presented in Figure 55. This reaction sequence is also consistent with the two-phased process which occurs in the respective binary systems at hyperstoichiometric compositions. Therefore, as shown in the proposed reaction sequence, the two, three-phased fields will run out to the respective binary systems with increasing temperature leaving behind a complete series of solid solutions of the disordered- $(\text{Nb}, \text{Ta})_2\text{C}$.

Because the transition in Nb_2C and Ta_2C at hypostoichiometric compositions does not involve a first-order phase change, no three-phase equilibria are expected to result in the order-disorder transformation at the metal-rich boundary of the subcarbide phase. The same is probably true for the displacive transformation which occurs in the Nb_2C binary phase at $\sim 1230^\circ\text{C}$. From the experimental results, the orthorhombic to hexagonal transition seems to be of a higher order type at both hypo- and hyperstoichiometric compositions.

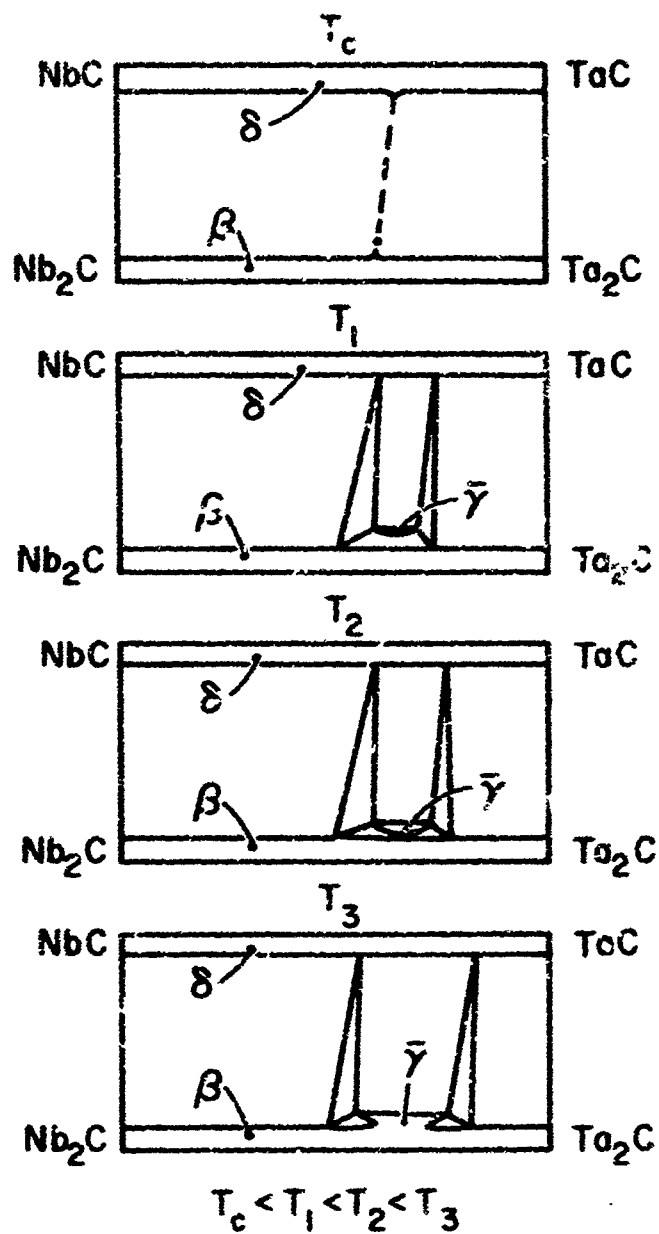


Figure 55. Nb-Ta-C: Schematic Illustration for the Formation of the $\bar{\gamma}$ -(Nb, Ta) $_2$ C $_{1+x}$ Phase: Disordered- $\bar{\gamma}$ -(Nb, Ta) $_2$ C $_{1+x} \rightleftharpoons$ Ordered- β -(Nb, Ta) $_2$ C + δ -(Nb, Ta) C_{1-x} .

To compare the experimental tie-line distributions in the two-phase fields of $(\text{Nb}, \text{Ta})-(\text{Nb}, \text{Ta})_2\text{C}_{1-x}$ and $(\text{Nb}, \text{Ta})_2\text{C}_{1-x}-(\text{Nb}, \text{Ta})\text{C}_{1-x}$ with the thermodynamically calculated values, one has to know the free enthalpies of formation of the binary phases at the respective carbon concentrations.

Tables 3 and 4 list the enthalpy differences which were used for the calculation of the tie-line distributions in the corresponding two-phase fields.

Using the assumptions of constant carbon concentrations and ideal solution behavior in the three series of solid solutions, the conditional equations governing the two-phase equilibria in the ternary system are:

$$\frac{\partial \Delta G_f(\text{Nb}, \text{Ta})\text{C}_v}{\partial x_{\text{Ta}}} = \frac{\partial \Delta G_f(\text{Nb}, \text{Ta})\text{C}_v}{\partial x_{\text{Ta}}} \quad \text{Eq (1)}$$

T, p

and

$$\frac{\partial \Delta G_f(\text{Nb}, \text{Ta})\text{C}_v}{\partial x_{\text{Ta}}'} = \frac{\partial \Delta G_f(\text{Nb}, \text{Ta})\text{C}_w}{\partial x_{\text{Ta}}''} \quad \text{Eq (2)}$$

T, p

Table 3. Free Enthalpy Data of Niobium Carbides

Phase	Free Energy of Formation (cal/gr-At. Nb)
$\text{NbC}_{0.75}$	$\Delta G_f = -28,185 + 0.755 T$
$\text{NbC}_{0.48}$	$\Delta G_f = -21,100$ (constant)
$\text{NbC}_{0.5}$	$\Delta G_f = -22,900$ (constant)

Table 4. Free Enthalpy Data of Tantalum Carbides

Phase	Free Energy of Formation (cal/gr-At. Ta)
$\text{TaC}_{0.75}$	$\Delta G_f = -26,943 + 0.88 T$
$\text{TaC}_{0.48}$	$\Delta G_f = -23,000$ (constant)
$\text{TaC}_{0.5}$	$\Delta G_f = -24,300$ (constant)

The thermodynamic evaluation of the phase equilibria at 1500 and 1800°C (Figures 56 and 57) was derived from the following free energy-concentration gradient curves.

Metal Solid Solution, Calculated for $u \sim 0$.

$$\left[\frac{\partial \Delta G_f(\text{Nb, Ta})C_u}{\partial x_{\text{Ta}}} \right]_{T, p} = RT \ln \left(\frac{x_{\text{Ta}}}{1-x_{\text{Ta}}} \right) \quad \text{Eq (3)}$$

Subcarbide Solid Solution, Calculated for $u \approx 0.48$ and 0.5.

$$\left[\frac{\partial \Delta G_f(\text{Nb, Ta})C_v}{\partial x'_{\text{Ta}}} \right]_{T, p} = \Delta G_{f\text{TaC}_v} - \Delta G_{f\text{NbC}_v} + RT \ln \left(\frac{x'_{\text{Ta}}}{1-x'_{\text{Ta}}} \right) \quad \text{Eq (4)}$$

Monocarbide Solid Solution, Calculated for $w \approx 0.75$.

$$\left[\frac{\partial \Delta G_v(\text{Nb, Ta})C_w}{\partial x''_{\text{Ta}}} \right]_{T, p} = \Delta G_{f\text{TaC}_w} - \Delta G_{f\text{NbC}_w} + RT \ln \left(\frac{x''_{\text{Ta}}}{1-x''_{\text{Ta}}} \right) \quad \text{Eq (5)}$$

where the x_{Ta} , x'_{Ta} , and x''_{Ta} values in the preceding equations represent the relative mole fractions of tantalum in the metal, subcarbide, and monocarbide solid solutions, respectively.

We may now compare the partition equilibrium constants (k) derived from the experimental sections at 1500 and 1800°C with the calculated values obtained from Equations 1 and 2.

Two-Phase Equilibrium (Nb, Ta)-(Nb, Ta) $C_{0.48}$

$$(u \sim 0, v \approx 0.48) \text{ where } K_{uv} = \frac{x'_{\text{Ta}}}{1-x'_{\text{Ta}}} \cdot \frac{1-x_{\text{Ta}}}{x_{\text{Ta}}}$$

$$\begin{aligned} 1500^\circ\text{C} \quad K_{\text{cal}} &= 1.71 \\ K_{\text{exp}} &= 1.79 \pm 0.11 \end{aligned}$$

Two-Phase Equilibrium $(\text{Nb, Ta})\text{C}_{0.5} - (\text{Nb, Ta})\text{C}_{0.75}$

$$(u \approx 0.5, w \approx 0.75) \text{ where } K_{vw} = \frac{x_{\text{Ta}}''}{1-x_{\text{Ta}}''} \cdot \frac{1-x_{\text{Ta}}'}{x_{\text{Ta}}'}$$

$$1800^{\circ}\text{C} \quad K_{\text{cal}} = 1.22$$

$$K_{\text{exp}} = 1.27 \pm 0.04$$

The uncertainties in the experimentally determined (K) values are a result of the scatter of values obtained from the individual tie lines.

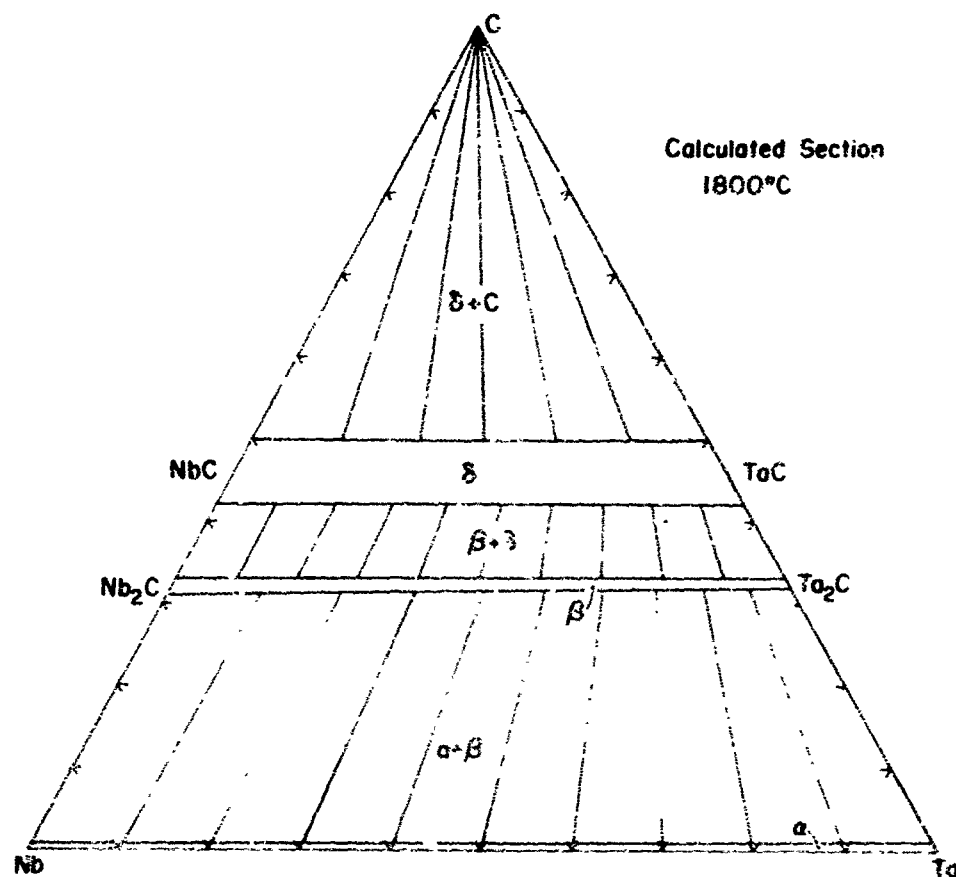


Figure 56. Nb-Ta-C: Calculated Section at 1800°C

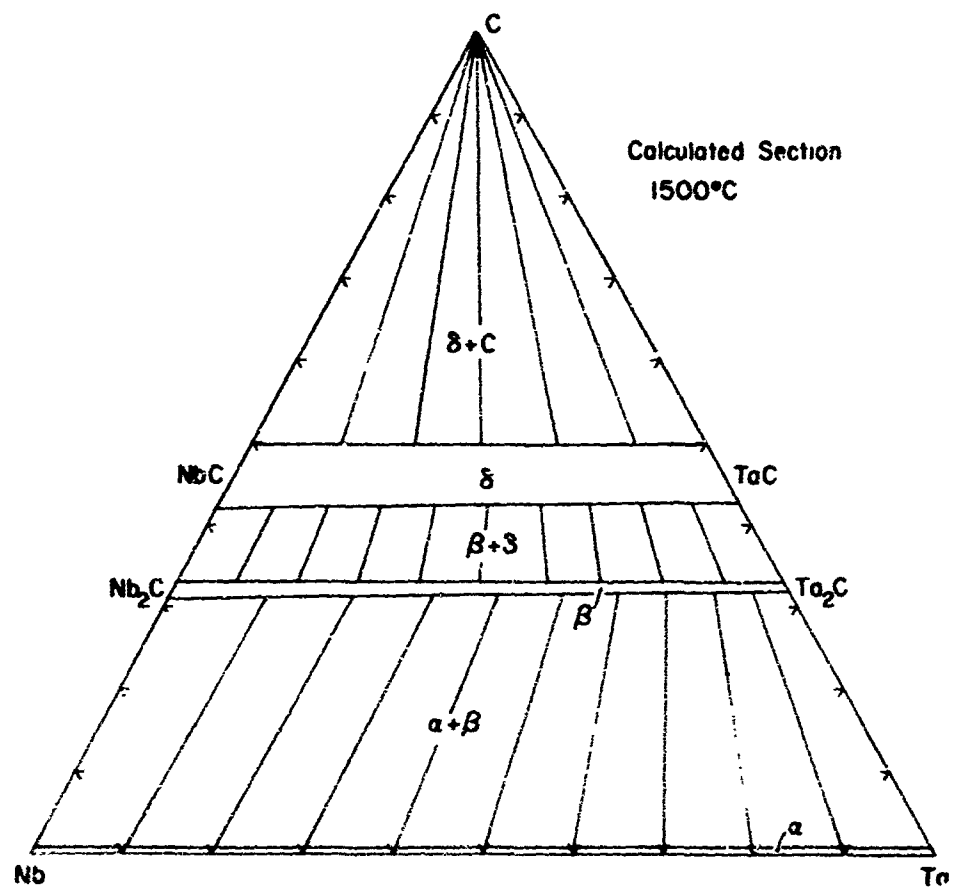


Figure 57. Nb-Ta-C: Calculated Section at 1500°C

REFERENCES

1. Bueckle, H.: Z. Metallk. 37 (1946) 53
2. Williams, D.E. and W.H. Pechin: Trans. ASM 50 (1958)1081
3. Storms, E.K. and N.H. Krikorian: J. Phys. Chem. 64 (1960)1471
4. Kimura, H. and Y. Sasaki: Trans. Jap. Inst. Met. 2 (1961)98
5. Rudy, E., S. Windisch, and C.E. Brukl: AFML-TR-65-2, Part I, Vol. XII (Sept. 1967)
6. Rudy, E. and C.E. Brukl: J. Amer. Ceram. Soc. 50 No. 5, (1967), 265
7. Terao, N.: Jap. J. Appl. Phys. 3 (1964), 104.
8. Volkova, N.M. and P.V. Gel'd: Izvest. Vysh. Uchebnik Zaved. Tsvetnaya Metallurgiya 3 (1965), 77.
9. Alyamovskii, S.I., G.P. Sheikin, and P.V. Gel'd, J. Neorg. Chim. 8 (1963), 2000.
10. Yvon, K., H. Nowotny, and R. Kieffer: Mh. Chem. 98 (1967), 34.
11. Rudy, E.: AFML-TR-65-2, Part II, Vol. VIII (March 1966), 105.
12. Rudy, E. and D.P. Harmon: AFML-TR-65-2, Part I, Vol. V (Jan. 1966).
13. Bowman, A.L., T.C. Wallace, J. L. Yarnell, R. G. Wenzel, and E. K. Storms: Acta Cryst. 19 (1965), 6
14. Lesser, R. and G. Brauer: Z. Metallkde. 49 (1958), 622.
15. Zaplatynsky, I.: J. Amer. Ceram. Soc. 49, No. 2 (1966), 109.
16. Brizes, W.F. and S.M. Tobin: J. Am. Ceram. Soc. 50 (1967), 115
17. Nowotny, H. and R. Kieffer: Z. Metallk. 38 (1947), 257
18. Norton, J.T. and A. L. Mowrv J. Metals 1 (1949) 133.
19. Agte, C. and H. Alterthum: Z. Tech. Physik 11 (1930) 182.
20. Rudy, E., St. Windisch, and Y.A. Chang: AFML-TR-65-2, Part I, Vol. I, (Jan. 1965).
21. Rudy, E. and G. Progulski: Planseeber. Pulvermet., 15, No. 1, p. 13 (1967).

REFERENCES (Cont)

22. Heetderks, H.D., E. Rudy, and T. E. Eckert: Planseeber. Pulvermet., 13, p. 105 (1965), also USAF Report AFML-TR-65-2, Part IV, Vol. 1 (1965).
23. Elliott, R. P.: Constitution of Binary Alloys, First Supplement, McGraw-Hill, New York (1965).
24. Pearson, W.B.: Handbook of Lattice Spacings and Structures of Metals, Pergamon Press, New York (1958).

UNCLASSIFIED

Security Classification

DOCUMENT CONTROL DATA - R & D		
(Security classification of title, body of abstract and indexing annotation must be entered when the overall report is classified)		
1. ORIGINATING ACTIVITY (Corporate author)		2a. REPORT SECURITY CLASSIFICATION
Materials Research Laboratory Aerojet-General Corporation Sacramento, California		Unclassified
		2b. GROUP
		N/A
3. REPORT TITLE		
Phase Equilibria Investigations of Binary, Ternary, and Higher Order Systems. Part III. The Nb-Ta-C System		
4. DESCRIPTIVE NOTES (Type of report and inclusive dates)		
5. AUTHOR(S) (First name, middle initial, last name)		
Booker, Phillip H. Rudy, Erwin		
6. REPORT DATE	7a. TOTAL NO. OF PAGES	7b. NO. OF REFS
April 1970	67	34
8a. CONTRACT OR GRANT NO.	8b. ORIGINATOR'S REPORT NUMBER(S)	
F33615-67-C-1513	None	
9. PROJECT NO.	9d. OTHER REPORT NO(S) (Any other numbers that may be assigned this report)	
7350	AFML-TR-69-117, Part III	
c. Task 735001		
4.		
10. DISTRIBUTION STATEMENT		
This document has been approved for public release and sale; its distribution is unlimited.		
11. SUPPLEMENTARY NOTES		12. SPONSORING MILITARY ACTIVITY
		Air Force Materials Laboratory (MANC) Wright-Patterson AFB, Ohio 45433
13. ABSTRACT		
<p>The solid state and solid-liquid equilibria of the Nb-Ta-C system have been determined by melting point determinations, X-ray and chemical analysis, metallography, and differential thermal analysis for temperatures above 1500°C.</p> <p>The ternary system has a complete solid solution of monocarbides and also of subcarbides if the differences in carbon atom ordering is disregarded. Eutectic troughs in both the metal-rich and carbon-rich regions of the ternary are present. Calculated tie-line distributions agree well with experimental results.</p>		

DD FORM 1 NOV 65 1473

Security Classification

Security Classification

14 KEY WORDS	LINK A		LINK B		LINK C	
	ROLE	WT	ROLE	WT	ROLE	WT
Phase Equilibria Cutting Tools Niobium-Tantalum-Carbon Thermodynamics						

Security Classification